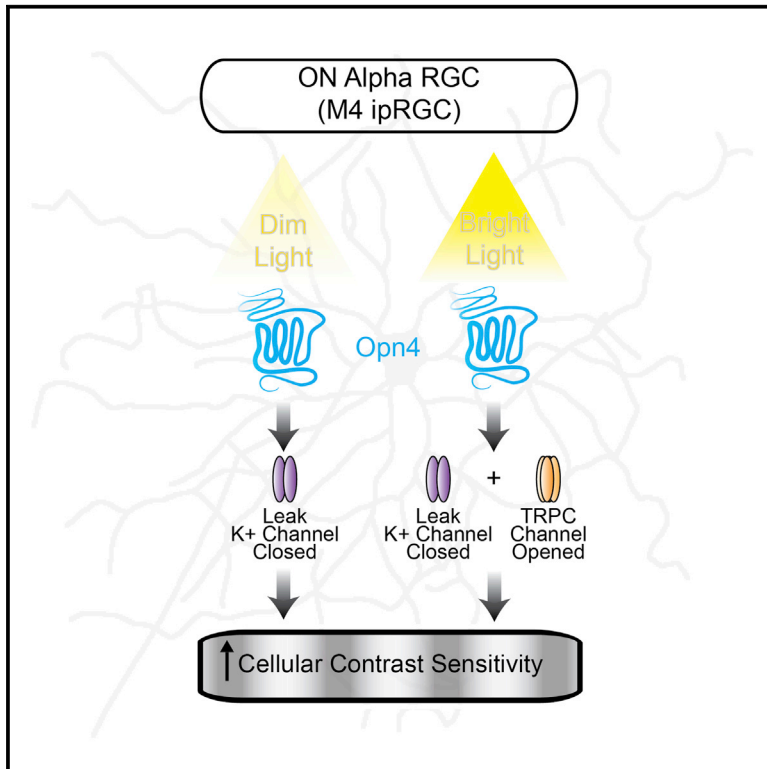


Neuron

Melanopsin Phototransduction Is Repurposed by ipRGC Subtypes to Shape the Function of Distinct Visual Circuits

Graphical Abstract



Authors

Takuma Sonoda, Seul Ki Lee,
Lutz Birnbaumer, Tiffany M. Schmidt

Correspondence

tiffany.schmidt@northwestern.edu

In Brief

Sonoda et al. identify leak potassium channels as the major target of melanopsin phototransduction in M4 ipRGCs/ON alpha retinal ganglion cells. Melanopsin-dependent closure of these channels enhances cell excitability and contrast sensitivity across a wide range of light intensities.

Highlights

- Melanopsin enhances contrast sensitivity of M4 ipRGCs (ON alpha cells)
- Melanopsin phototransduction increases M4 ipRGC intrinsic excitability
- Melanopsin phototransduction closes leak potassium channels in M4 ipRGCs
- Melanopsin modulates M4 ipRGC physiology across a wide range of light intensities



Melanopsin Phototransduction Is Repurposed by ipRGC Subtypes to Shape the Function of Distinct Visual Circuits

Takuma Sonoda,^{1,2} Seul Ki Lee,¹ Lutz Birnbaumer,^{3,4} and Tiffany M. Schmidt^{1,5,*}

¹Department of Neurobiology, Northwestern University, Evanston, IL, USA

²Northwestern University Interdepartmental Neuroscience Program, Northwestern University, Chicago, IL, USA

³Neurobiology Laboratory, National Institute of Environmental Health Sciences, National Institutes of Health, Durham, NC, USA

⁴Institute of Biomedical Research (BIOMED), School of Medical Sciences, Catholic University of Argentina, Buenos Aires, Argentina

⁵Lead Contact

*Correspondence: tiffany.schmidt@northwestern.edu

<https://doi.org/10.1016/j.neuron.2018.06.032>

SUMMARY

Melanopsin is expressed in distinct types of intrinsically photosensitive retinal ganglion cells (ipRGCs), which drive behaviors from circadian photoentrainment to contrast detection. A major unanswered question is how the same photopigment, melanopsin, influences such vastly different functions. Here we show that melanopsin's role in contrast detection begins in the retina, via direct effects on M4 ipRGC (ON alpha RGC) signaling. This influence persists across an unexpectedly wide range of environmental light levels ranging from starlight to sunlight, which considerably expands the functional reach of melanopsin on visual processing. Moreover, melanopsin increases the excitability of M4 ipRGCs via closure of potassium leak channels, a previously unidentified target of the melanopsin phototransduction cascade. Strikingly, this mechanism is selective for image-forming circuits, as M1 ipRGCs (involved in non-image forming behaviors), exhibit a melanopsin-mediated decrease in excitability. Thus, melanopsin signaling is repurposed by ipRGC subtypes to shape distinct visual behaviors.

INTRODUCTION

Intrinsically photosensitive retinal ganglion cells (ipRGCs) respond directly to light because they express the photopigment melanopsin (Berson et al., 2002; Hattar et al., 2002). There are five subtypes of ipRGC, which mediate vastly different behaviors from non-image forming functions such as circadian photoentrainment (M1 ipRGCs) to contrast sensitivity in image formation (M2-M5 ipRGCs) (Güler et al., 2008; Hatori et al., 2008; Schmidt et al., 2014). The intrinsic, melanopsin phototransduction cascade of ipRGCs encodes environmental light levels over multiple seconds, while the canonical rod and cone photoreceptors relay rapid, spatially discrete information about the visual scene

to retinal ganglion cells with millisecond precision. ipRGCs are unique among retinal ganglion cells in that they integrate rod, cone, and melanopsin signals before relaying light information to downstream targets in the brain (Schmidt and Kofuji, 2010; Wong et al., 2007; Zhao et al., 2014).

The slow timescale over which melanopsin phototransduction occurs has led to the widespread belief that this component of ipRGC signaling is mainly important for subconscious, non-image forming behaviors (Berson et al., 2002; Güler et al., 2008; Hattar et al., 2002; Lucas et al., 2003; Ruby et al., 2002; Schmidt et al., 2011). However, our recent behavioral evidence points to a surprising, and critical, role for melanopsin phototransduction in image-forming (pattern) vision, raising the question of how ipRGCs integrate temporally and functionally distinct rod/cone and melanopsin-based signals to influence this behavior (Schmidt et al., 2014; Sonoda and Schmidt, 2016). Complicating interpretation of these findings is the fact that melanopsin phototransduction in the ipRGC subtypes most likely involved in pattern vision, M2-M5 ipRGCs, has been reported to activate a slow, small photocurrent only at bright, photopic light intensities (Ecker et al., 2010; Estevez et al., 2012; Schmidt and Kofuji, 2009; Zhao et al., 2014). These reports call into question the potential physiological relevance of melanopsin signaling in M2-M5 ipRGCs. This use of small M2-M5 melanopsin photocurrent amplitude as a proxy for its functional significance relies on the assumption that melanopsin phototransduction acts on identical intracellular targets in all ipRGC subtypes. However, melanopsin phototransduction has only been well-studied in M1 (non-image forming) ipRGCs, where it has been shown to activate a Gq cascade leading to depolarization via opening of transient receptor potential 6 and 7 (TRPC 6/7) channels (Graham et al., 2008; Hartwick et al., 2007; Perez-Leighton et al., 2011; Warren et al., 2006; Xue et al., 2011). The diverse physiological properties, central projections, and behavioral roles of individual ipRGC subtypes suggest that it may be advantageous for melanopsin phototransduction to employ different mechanisms of action across ipRGC subtypes (Ecker et al., 2010; Schmidt and Kofuji, 2009, 2011; Schmidt et al., 2011, 2014; Sonoda and Schmidt, 2016). This would allow for image-forming ipRGC subtypes to modulate how rod and cone signals are integrated to influence pattern vision in unexpected ways.



In this work, we directly address two outstanding questions in the field: what are the physiological consequences of melanopsin phototransduction on visual signaling within ipRGCs themselves? And, are the transduction targets of melanopsin identical across ipRGC subtypes? We find that melanopsin phototransduction enhances the contrast sensitivity of M4 ipRGCs (ON alpha RGCs, which are involved in pattern vision) (Schmidt et al., 2014) across a surprisingly wide range of light intensities from bright, photopic (12 log quanta/cm²/s) to dim, scotopic light levels (9 log quanta/cm²/s) where only rod phototransduction was thought to drive vision. Melanopsin phototransduction achieves this influence through increasing the excitability of M4 ipRGCs via a previously unidentified modulation of potassium leak channels. These mechanisms are unique to image forming visual circuits because melanopsin phototransduction differentially modulates the intrinsic excitability of M1 ipRGCs, which are known to be involved in non-image forming, subconscious visual behaviors. Collectively, our results show that melanopsin's contribution to vision arises from a direct effect on M4 ipRGC signaling within the retina and demonstrate that melanopsin phototransduction is repurposed in ipRGC subtypes to shape distinct visual behaviors.

RESULTS

Melanopsin Enhances the Contrast Sensitivity of M4 Cells

We have previously reported that melanopsin null (*Opn4*^{-/-}) animals exhibit reduced behavioral contrast sensitivity (Schmidt et al., 2014). However, where in the visual pathway these deficits originate is unknown. We therefore first investigated whether *Opn4*^{-/-} ipRGCs have reduced contrast sensitivity. We chose to focus on M4 cells (which are ON alpha RGCs) because they are highly sensitive to contrast and are one of the three major ipRGC subtypes (along with M2 and M5 cells) projecting to the dorsal lateral geniculate nucleus of the thalamus (dLGN) (Ecker et al., 2010; Estevez et al., 2012; Grimes et al., 2014; Stabio et al., 2018; Zaghoul et al., 2003). We measured the contrast sensitivity of M4 cells in WT and *Opn4*^{-/-} animals to drifting sine-wave gratings of an empirically determined optimum spatial frequency (0.04 c/d, Figures S1A and S1B) from bright, photopic (12 log quanta/cm²/s) to dim, scotopic mean light intensities (9 log quanta/cm²/s) 100-fold lower than the lowest reported threshold for melanopsin signaling in M4 cells (Figure 1A) (Schmidt et al., 2014). Surprisingly, *Opn4*^{-/-} M4 cells exhibited reduced contrast sensitivity even at the lowest light intensity tested, as evidenced by a significantly increased C₅₀ at all light levels (Figures 1B and 1C). Moreover, the contrast gain was significantly reduced in *Opn4*^{-/-} M4 cells at the two highest light intensities tested (Figure 1C). We also measured the contrast sensitivity of M4 cells to drifting gratings with a spatial frequency of 0.089 c/d, which is the spatial frequency at which we previously reported behavioral deficits in contrast sensitivity using the visual cortex-dependent visual water task (Prusky and Douglas, 2004; Schmidt et al., 2014). At this spatial frequency, we also saw significantly reduced contrast sensitivity of *Opn4*^{-/-} M4 cells at bright light levels (12 log quanta/cm²/s) (Figures 1D and 1E). These findings indicate that contrast sensitivity deficits in melanopsin null animals are first detectable within ipRGCs.

Activation of Gq Signaling Rescues Contrast Sensitivity Deficits in *Opn4*^{-/-} M4 Cells

Germline knockout of melanopsin was previously shown to affect retinal development (Rao et al., 2013). This raises the possibility that germline knockout of melanopsin could affect retinal circuit formation or function, causing the contrast sensitivity deficits in *Opn4*^{-/-} M4 cells. To address this possibility, we designed an experiment to selectively and acutely restore Gq signaling (the pathway endogenously activated by melanopsin; Graham et al., 2008) in ipRGCs using Gq-DREADDs. We used adeno-associated viral vectors to express Gq-DREADDs in ipRGCs in *Opn4*^{Cre/Cre} (melanopsin null) retinas via intravitreal injection (Figure 2A). We then acutely applied 10 nM clozapine-N-oxide (CNO), which activated the Gq cascade in *Opn4*^{Cre/Cre} M4 cells to levels that matched melanopsin-mediated Gq activation in WT M4 cells under bright light conditions, allowing us to compare chemogenetic versus melanopsin activation of the Gq pathway (Figures 2B and 2C). Chemogenetic activation of the Gq pathway restored contrast sensitivity of *Opn4*^{Cre/Cre} M4 cells to WT levels (Figures 2D and 2E). To further demonstrate that retinal circuitry is normal in *Opn4*^{-/-} retinas, we measured the contrast sensitivity of a non-melanopsin-expressing RGC type (OFF alpha RGCs) and found no differences between WT and *Opn4*^{-/-} (Figures S1G and S1H). Additionally, WT and *Opn4*^{-/-} M4 cell morphology, spatial frequency tuning, and excitatory synaptic inputs were identical (Figures S1A–S1F). Collectively, these data indicate that the contrast sensitivity deficits observed in *Opn4*^{-/-} M4 cells do not arise from circuit rewiring due to germline knockout of melanopsin, but rather from direct action of the intracellular melanopsin phototransduction cascade on M4 cell signaling.

Melanopsin Phototransduction Modulates the Membrane Potential and Resting Spike Rate of M4 Cells at Scotopic Light Intensities

How can melanopsin phototransduction, which has previously been reported to be activated at only bright, photopic light intensities, influence contrast sensitivity at dim light intensities where rod signaling is thought to predominate? Previous measurements of melanopsin phototransduction thresholds in M4 cells were made using relatively brief stimuli in light adapted or melanopsin heterozygous retinas (Schmidt et al., 2014; Estevez et al., 2012; Zhao et al., 2014). However, melanopsin phototransduction is capable of integrating light information over minutes and hours (Do and Yau, 2013; Schmidt et al., 2014; Wong, 2012). We reasoned that the slow integration time and sustained nature of melanopsin phototransduction may actually depolarize and increase the resting spike rate of M4 cells during more physiological conditions of tonic exposure to even dim background light. These effects could, in turn, enhance the M4 cell response to rod and cone inputs relayed near contrast threshold to enhance contrast sensitivity. We therefore measured the steady-state firing rate and resting membrane potential (V_m) of M4 cells in constant background light from 9 to 12 log quanta/cm²/s. WT M4 cells showed significantly elevated spike rates and V_m compared to *Opn4*^{-/-} M4 cells, even at the lowest light intensity tested (Figures 3A–3D and S2). This elevated V_m was also observed when action potentials were blocked via inclusion

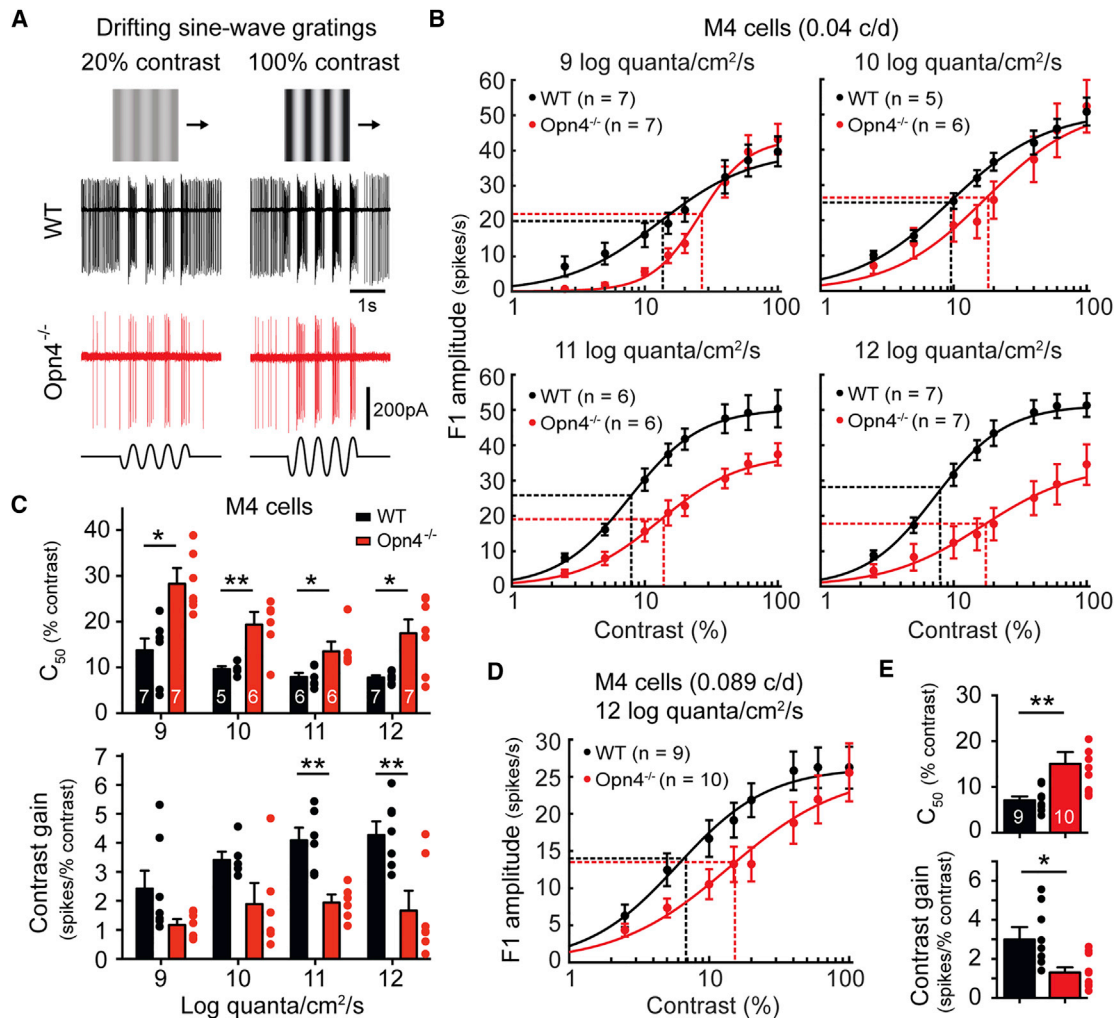


Figure 1. Melanopsin Enhances the Contrast Sensitivity of M4 Cells/ON-Alpha RGCs across a Wide Range of Physiological Light Levels

(A) Example loose-patch recordings of WT (black) and *Opn4*^{-/-} (red) M4 cell responses to drifting sine-wave gratings of 20% (left) or 100% (right) contrast in bright (12 log quanta/cm²/s) background light. *Ex vivo* retinas were presented with drifting sine-wave gratings of an empirically determined optimum spatial frequency (0.04 cycles/degree, Figure S1) of varying contrast.

(B) Contrast response functions of M4 cells in WT (black) and *Opn4*^{-/-} (red) retinas recorded at background light levels from 9 to 12 log quanta/cm²/s. Vertical dotted lines indicate C_{50} and horizontal dotted lines indicate half-maximal response.

(C) C_{50} and contrast gain of WT (black) and *Opn4*^{-/-} (red) M4 cells at background light levels from 9 to 12 log quanta/cm²/s.

(D) Contrast response functions of M4 cells in WT (black) and *Opn4*^{-/-} (red) retinas recorded in response to drifting sine-wave gratings with a spatial frequency of 0.089 cycles/degree. Recordings were made at bright background light levels (12 log quanta/cm²/s).

(E) C_{50} and contrast gain of WT (black) and *Opn4*^{-/-} (red) M4 cells in response to drifting gratings with a spatial frequency of 0.089 cycles/degree.

All data are mean \pm SEM. * $p < 0.05$. ** $p < 0.01$.

of the voltage-gated sodium channel blocker QX-314 in the internal solution (Figure 3D). We then pharmacologically isolated the intrinsic, melanopsin-based response of M4 cells with a cocktail of synaptic blockers and found that melanopsin phototransduction alone significantly depolarized the membrane potential of M4 cells in 10 min of background light from 10 to 12 log quanta/cm²/s (Figures 4A–4C). However, at 9 log quanta/cm²/s, we did not see a significant depolarization from baseline in the absence of synaptic input.

We next attempted to detect melanopsin-dependent depolarization in the nucleated patch configuration in response to a dim,

9 log quanta/cm²/s light stimulus. In this configuration, we were able to detect a small, but consistent, melanopsin-based depolarization even at 9 log quanta/cm²/s (3.39 ± 0.50 mV, $n = 5$ cells), likely due to the small membrane compartment and consequent higher input resistance of a nucleated patch (Figure 4D). These findings allow us to rule out any possibility that the dim light, melanopsin-mediated response of M4 cells is a result of electrical coupling. Collectively, these data show that melanopsin phototransduction is active and sets M4 cell V_m and spike rate across the full range of light intensities over which we observed cellular contrast sensitivity deficits in *Opn4*^{-/-} M4 cells.

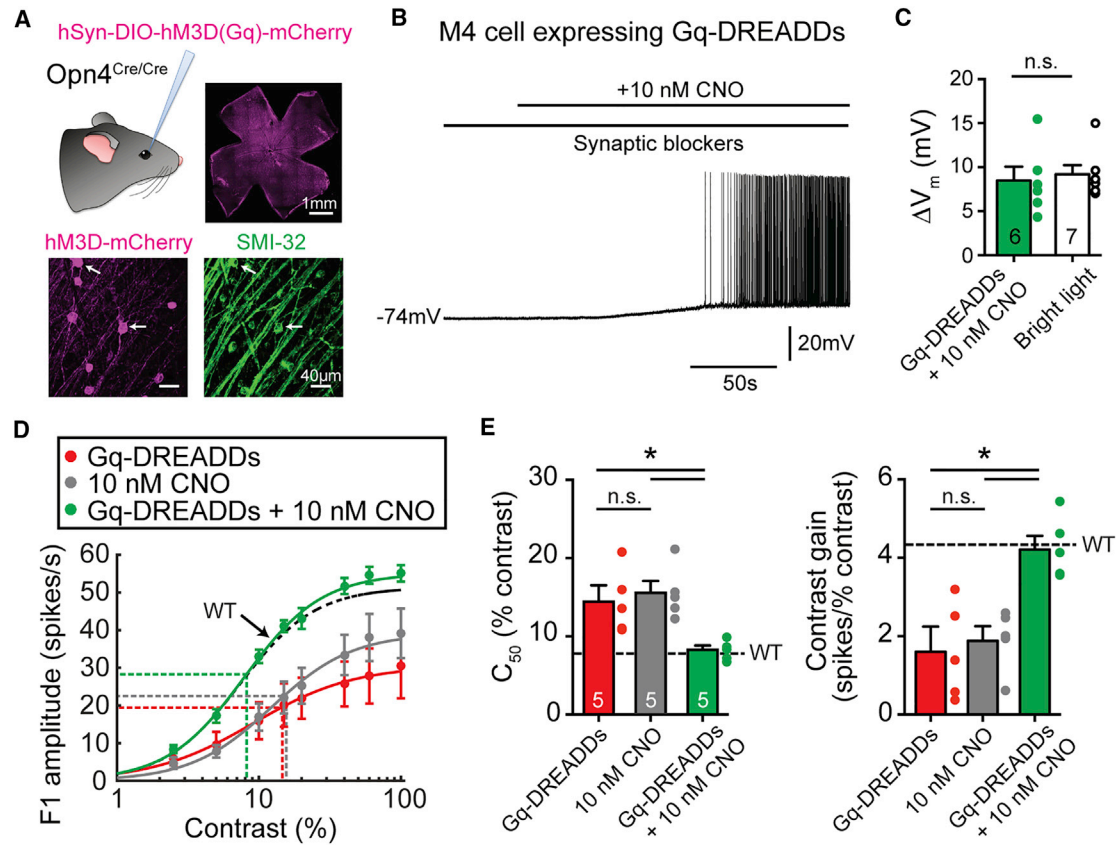


Figure 2. Activation of the Gq Cascade Using Gq-DREADDs Rescues Contrast Sensitivity Deficits in *Opn4*^{-/-} M4 Cells

(A) Gq-DREADDs were expressed in ipRGCs of melanopsin null (*Opn4*^{Cre/Cre}) mice via intravitreal injections of AAV2/hSyn-DIO-hM3D-mCherry (Gq-DREADDs). Top right panel shows successful transfection of ipRGCs across the retina. Bottom panels show mCherry immunostaining of Gq-DREADD-positive ipRGCs (magenta) and SMI-32 immunostaining (green), which strongly labels alpha RGCs. White arrows indicate putative M4 cells expressing Gq-DREADDs.

(B) Whole-cell current-clamp recording of a Gq-DREADD-expressing M4 cell in an *Opn4*^{Cre/Cre} retina exposed to 10 nM CNO in the dark in the presence of synaptic blockers.

(C) 10 nM CNO elicited a membrane potential depolarization of 8.48 ± 1.58 mV in *Opn4*^{Cre/Cre} M4 cells expressing Gq-DREADDs in the dark (green), similar to light-evoked depolarization of 9.20 ± 1.02 mV in WT M4 cells (white) in bright (12 log quanta/cm²/s) light (Figure 4C).

(D) Contrast response functions of M4 cells under bright (12 log quanta/cm²/s) background illumination in melanopsin null (*Opn4*^{Cre/Cre}) M4 cells infected with Gq-DREADDs but not exposed to CNO (red), not infected with Gq-DREADDs but exposed to 10 nM CNO (gray), or infected with DREADDs and exposed to 10 nM CNO (green). Dotted black line indicates contrast response function of WT M4 cells in bright (12 log quanta/cm²/s) background light (Figure 1B).

(E) C_{50} and contrast gain of M4 cells in (D). Black dotted line indicates WT values recorded in bright (12 log quanta/cm²/s) light from Figure 1C.

All data are represented as mean \pm SEM. * $p < 0.05$. ** $p < 0.01$. n.s., not significant. CNO, clozapine-N-oxide.

Melanopsin Enhances the Intrinsic Excitability of M4 Cells

Melanopsin phototransduction increases the resting spike rate of M4 cells at 9 log quanta/cm²/s, a light intensity at which melanopsin phototransduction alone is not sufficient to depolarize V_m in intact cells (Figures 3 and 4). This suggests that melanopsin phototransduction has additional influences on M4 cell physiology beyond directly depolarizing V_m . The Gq cascade has been reported to alter intrinsic excitability of cells in systems outside of the retina and therefore could potentially exert similar effects in M4 cells (Brown and Passmore, 2009; Feliciangeli et al., 2015; Greene and Hoshi, 2017; Mathie, 2007). To test this, we assessed the intrinsic excitability of M4 cells by measuring evoked firing in darkness versus background light. WT M4 cells were held at a subthreshold membrane potential

of approximately -75 mV in current-clamp mode and bathed in a cocktail of synaptic blockers to isolate melanopsin-mediated effects on intrinsic excitability. We then injected positive current and measured spike output to each current injection in darkness and then in background light from 9 to 12 log quanta/cm²/s. We found that background light enhanced the intrinsic excitability of M4 cells at all intensities tested (Figures 5A–5C). This increase in excitability was melanopsin dependent because background light did not increase the excitability of *Opn4*^{-/-} M4 cells (Figures S3A and S3B). Background light also failed to alter the excitability of non-melanopsin-expressing, OFF alpha RGCs (Figures S3C and S3D).

To test whether acute activation of the Gq pathway in melanopsin null (*Opn4*^{Cre/Cre}) M4 cells was sufficient to enhance intrinsic excitability, we measured the excitability of

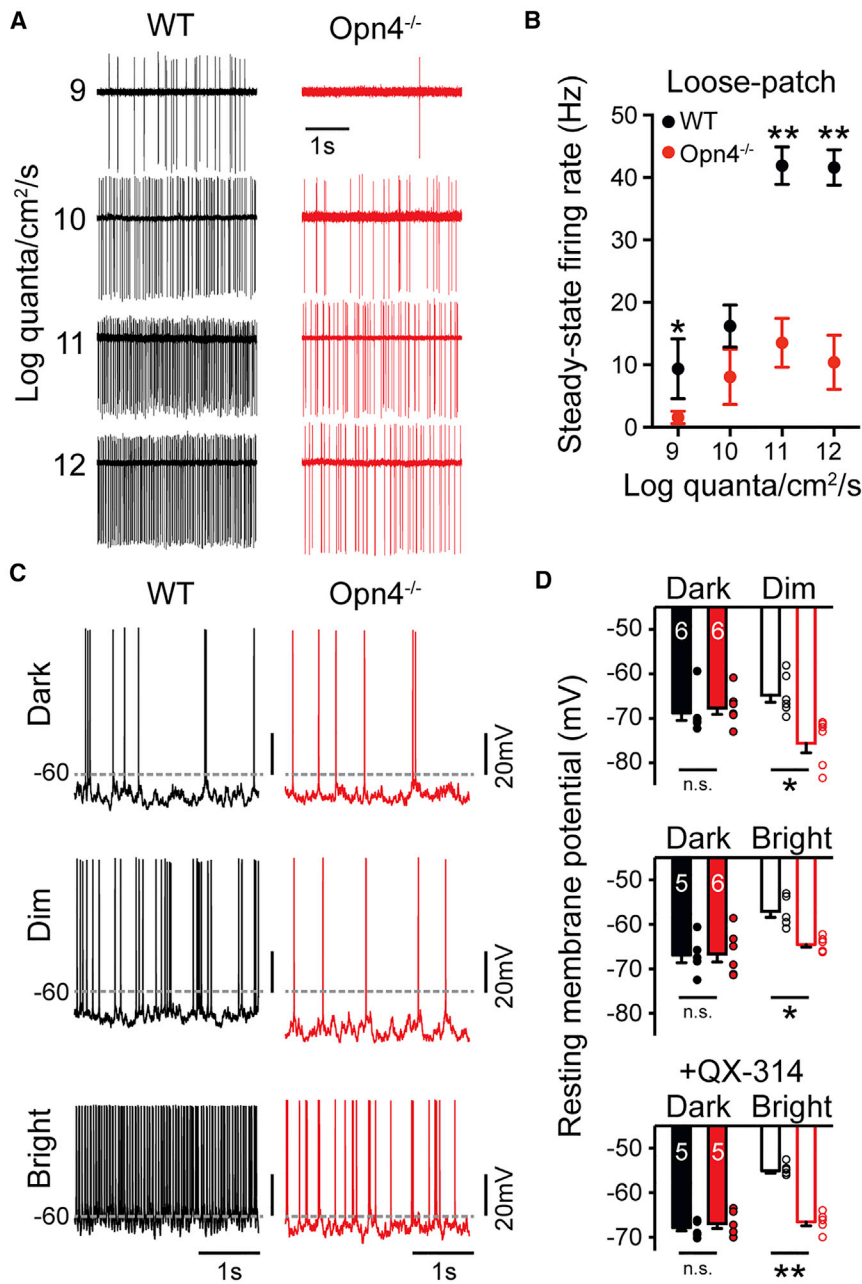


Figure 3. Melanopsin Increases the Steady-State Firing Rate and Resting Membrane Potential of M4 Cells across a Wide Range of Physiological Light Levels

(A) Example loose-patch recordings from WT (black) and *Opn4*^{-/-} (red) M4 cells in background light from 9 to 12 log quanta/cm²/s.

(B) Steady-state firing rate of WT (black) and *Opn4*^{-/-} (red) M4 cells measured with loose-patch recordings after 5–10 min in background light ($n = 5$ –7 cells/group, same cells as Figures 1B and 1C).

(C) Whole-cell recordings from WT (black) and *Opn4*^{-/-} (red) M4 cells in darkness and in dim (9 log quanta/cm²/s) or bright (12 log quanta/cm²/s) background light. Dotted gray lines indicate value of -60 mV.

(D) V_m of WT (black) and *Opn4*^{-/-} (red) M4 cells in darkness and after 5–10 min of dim (9 log quanta/cm²/s) or bright (12 log quanta/cm²/s) background illumination. WT M4 cells were significantly more depolarized in background light than *Opn4*^{-/-} cells. V_m was measured in the dark and then in dim or bright background light in the same cell. In a separate set of experiments, 2 mM QX-314 was included in the intracellular solution to measure resting membrane potential in the absence of spiking (bottom graph).

All data are represented as mean \pm SEM. * $p < 0.05$. ** $p < 0.01$. n.s., not significant. V_m , resting membrane potential.

Gq-DREADD-infected *Opn4*^{Cre/Cre} M4 cells in darkness before and after acute bath application of 10 nM CNO to mimic the Gq activation by melanopsin phototransduction in bright light (see Figures 2B and 2C). Gq activation alone was sufficient to enhance M4 cell excitability to levels similar to those seen in background light in WT M4 cells (Figures 5E and 5F). We next sought to determine whether it was possible to enhance cellular excitability via acute activation of the Gq cascade at levels that do not directly depolarize M4 cell V_m , mimicking the effects of melanopsin phototransduction in dim light. We identified 100 pM CNO as a concentration where we observed no change in the V_m of *Opn4*^{Cre/Cre} M4 cells expressing Gq-DREADDs, similar to

the lack of direct melanopsin-dependent depolarization in dim light (9 log quanta/cm²/s) (Figure 5D). We found that application of 100 pM CNO in darkness in the presence of synaptic blockers resulted in identical increases in the intrinsic excitability of Gq-DREADD-expressing *Opn4*^{Cre/Cre} M4 cells to that seen in 10 nM CNO (Figures 5E and 5F). Collectively, these data show that activation of endogenous Gq-coupled pathways by melanopsin increases intrinsic excitability. Moreover, our data using 100 pM CNO suggest that even a small amount of Gq activation can result in major changes in M4 cell excitability.

We next asked what physiological changes underlie melanopsin-dependent changes in M4 cell excitability. To test for the contribution of fast conductances, we compared action potential threshold, half-width, afterdepolarization (ADP) amplitude, and rate of decline in instantaneous firing rate and found no changes when M4 cells were exposed to background light compared to darkness (Figures S4A–S4D). These data suggest that modulation of fast conductances (e.g., Nav, BK, SK, Kv1, Kv3, Kv4, and Kv7) does not account for melanopsin-mediated increases in M4 cell excitability.

We next tested the possibility that melanopsin phototransduction causes an increase of input resistance (R_{inp}) through a

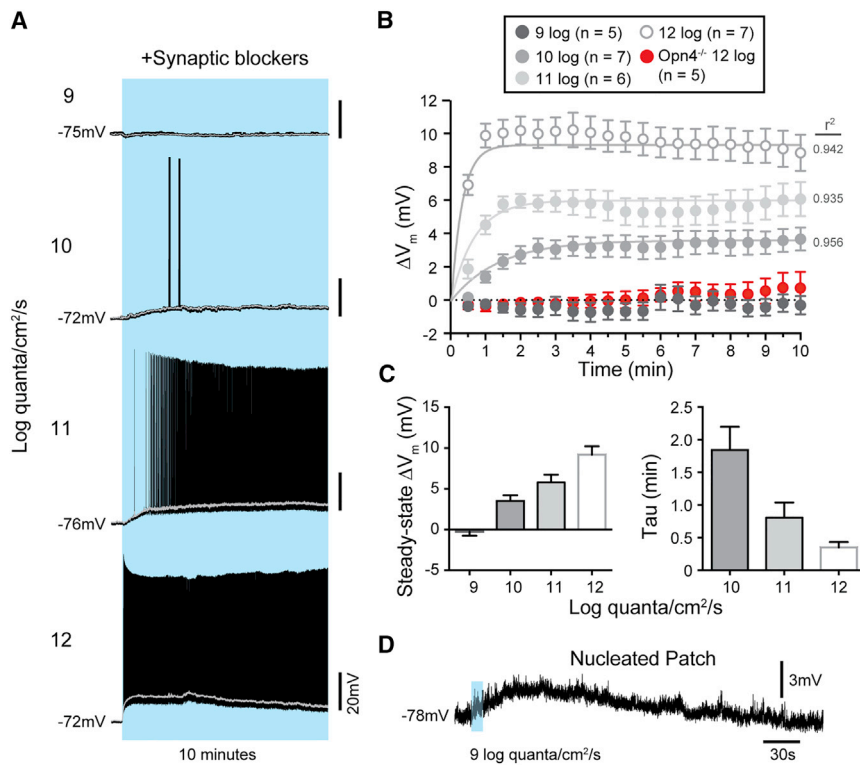


Figure 4. Melanopsin Phototransduction Directly Depolarizes M4 Cells across a Wide Range of Physiological Light Levels

(A) Example current-clamp recordings of WT M4 cell light responses to a 10 min, full-field background light ranging from 9 to 12 log quanta/cm²/s in a cocktail of synaptic blockers. Example traces are each from different cells. Gray lines represent traces filtered using a 1 s moving average.

(B) Mean ± SEM change in membrane potential (ΔV_m) from baseline in 30 s bins over 10 min of exposure to background light ranging from 9–12 log quanta/cm²/s. Dotted line indicates 0 mV change from baseline. Sustained, melanopsin-dependent depolarization was visible from 10–12 log quanta/cm²/s.

(C) Mean ± SEM steady-state ΔV_m (calculated as the average ΔV_m from baseline in the last 3 min of the light stimulus) and Tau (measured by fitting responses with a single exponential decay function, V_m(time) = (steady-state ΔV_m)(1 - e^{-time/tau})) at each light intensity.

(D) Example current-clamp recording from a nucleated M4 cell in response to a 10 s dim light stimulus (9 log quanta/cm²/s). Nucleated M4 cells exhibited an average peak depolarization of 3.39 ± 0.50 mV (n = 5 cells).

decrease in leak conductance in M4 cells. To test this, we measured R_{inp} of M4 cells in darkness and bright background light and found that the R_{inp} increased by ~20% (Figure S4G). Since the current-firing rate relationship of M4 cells is the same in dim and bright background light, we would expect R_{inp} increases to be the same in dim light. In support of this, when we measured R_{inp} of M4 cells in darkness compared to dim background light, we found a similar ~20% increase in R_{inp} (Figure S4G). In support of this, injection of both hyperpolarizing and depolarizing current steps in M4 cells in bright background light in the presence of synaptic blockers and TTX resulted in larger changes in V_m compared to darkness, pointing to a melanopsin-dependent decrease in a leak conductance (Figures S4E and S4F). Collectively, these results show that background light increases R_{inp} in M4 cells, which leads to increased intrinsic excitability.

Melanopsin phototransduction has previously been shown in M1 cells to activate a Gq-coupled pathway that results in the opening of TRPC 6/7 channels, which would lead to a decrease in R_{inp}. Therefore, the effects of background light on M4 cell physiology are inconsistent with the phototransduction cascade identified in M1 cells. This led us to question whether melanopsin phototransduction has differential effects on the intrinsic excitability of other ipRGC subtypes specialized for different behaviors again using evoked firing as a measure of intrinsic excitability. We tested this in M1 cells, which are involved in subconscious visual behaviors such as circadian photoentrainment and the pupillary light reflex but are not required for pattern vision (Güler et al., 2008; Schmidt et al., 2014). We targeted M1 cells in *Opn4*-GFP mice for current-clamp recording under two-photon excitation. We found that, unlike M4 cells, the intrinsic excitability

of M1 cells decreased in background light (Figures 6A–6C). This effect was consistent across M1 cells despite large biophysical diversity in the M1 cell population (Emanuel et al., 2017; Milner and Do, 2017). This decrease in intrinsic excitability was melanopsin dependent because it was absent in *Opn4*^{-/-} M1 cells (Figures 6B and 6C).

Potassium Leak Channels Are the Major Target of the Melanopsin Phototransduction Cascade in M4 Cells

The differential effects on M1 versus M4 cell intrinsic excitability suggest that melanopsin targets distinct conductances in M1 and M4 ipRGCs. If this is the case, then melanopsin-mediated currents in M1 and M4 cells should have distinct current-voltage (I-V) relationships. We therefore measured the I-V relationship of the light response of M1 and M4 cells (Figures 7A–7D). As expected, the maximum melanopsin-mediated current in M1 cells reversed near 0 mV, indicating that melanopsin activates a non-specific cationic conductance (Perez-Leighton et al., 2011; Warren et al., 2003; Xue et al., 2011) (Figures 7A and 7B). This current was abolished in *Trpc3*^{-/-}; *Trpc6*^{-/-}; *Trpc7*^{-/-} (TRPC 3/6/7 KO) retinas (Figures 7A and 7B), which is consistent with previous reports demonstrating that TRPC 6 and 7 channels are necessary for a melanopsin-dependent light response in M1 cells (Perez-Leighton et al., 2011; Xue et al., 2011).

In contrast, the melanopsin photocurrent in M4 cells exhibited a negative slope I-V relationship that reversed near -90 mV, (Figures 7C and 7D), which is very close to the equilibrium potential of potassium (E_k) in our preparation (-91.4 mV). The melanopsin-mediated current in M4 cells exhibited slow deactivation kinetics, which took over 10 min to return to baseline after light

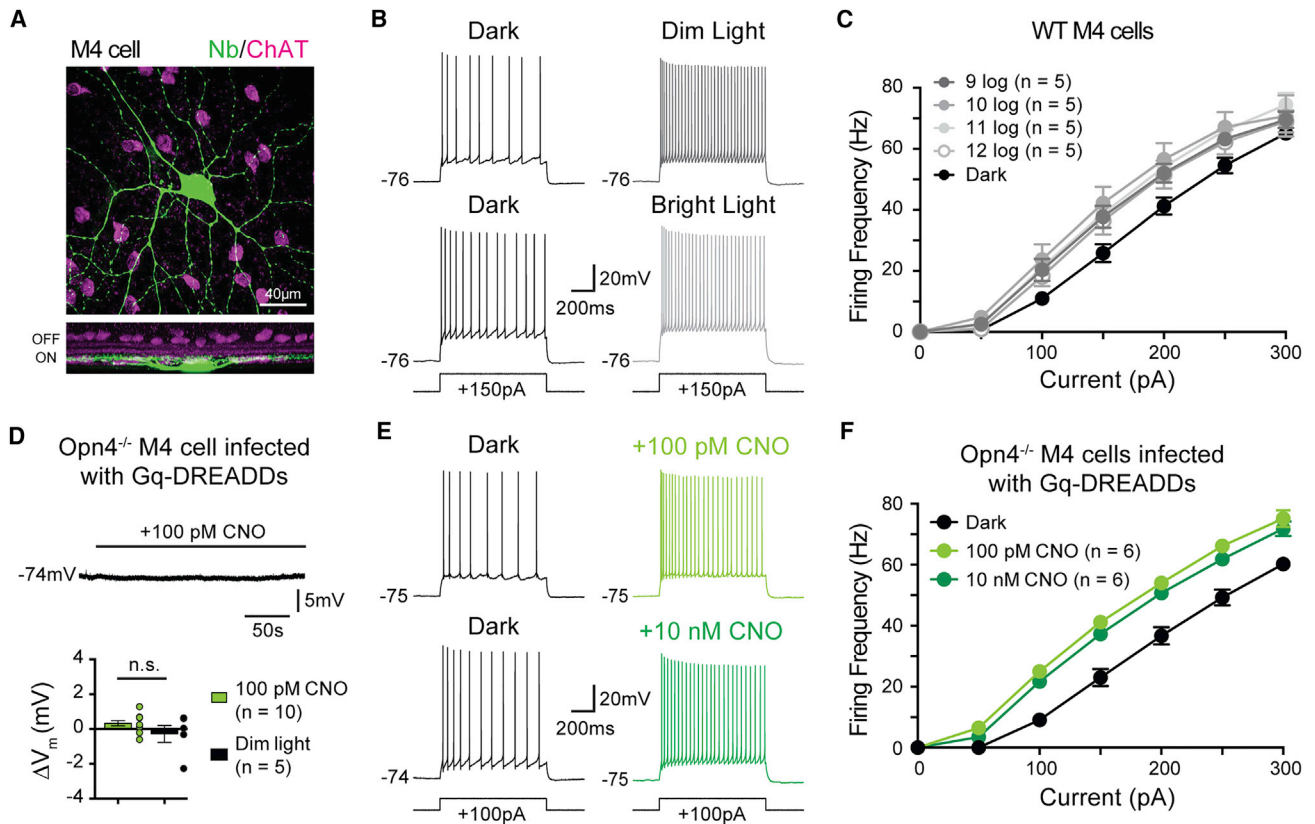


Figure 5. Melanopsin Increases the Intrinsic Excitability of M4 Cells from Scotopic to Photopic Light Levels

(A) Z stack, confocal image of an M4 cell filled with Neurobiotin (Nb, green) in retina co-immunolabeled for ChAT (magenta). Bottom panel shows a Z-projected view of the same cell in the orthogonal plane.

(B) Whole-cell recording of WT M4 cells in response to a 150 pA current injection in darkness (left panels) and in dim (9 log quanta/cm²/s top) or bright (12 log quanta/cm²/s bottom) background illumination (right panels).

(C) Firing rate plotted as a function of current injected in WT M4 cells at background illumination from 9 to 12 log quanta/cm²/s. Average dark firing rates for all cells are plotted in black. Spike output was higher in background illumination than in darkness at all light levels tested.

(D) Whole-cell current-clamp recording of Gq-DREADD-expressing M4 cell in an *Opn4^{Cre/Cre}* retina exposed to 100 pM CNO in the dark in the presence of synaptic blockers. CNO application did not elicit depolarization, mimicking lack of depolarization in dim background light (dim light data re-plotted from Figure 4C).

(E) Whole-cell recording of melanopsin null (*Opn4^{Cre/Cre}*) M4 cells infected with Gq-DREADDs in response to a 100 pA current injection in darkness before (black) and after either 100 pM (light green, top) or 10 nM (dark green, bottom) CNO application.

(F) Firing rate plotted as a function of current injected into melanopsin null (*Opn4^{Cre/Cre}*) M4 cells infected with Gq-DREADDs in the absence (black) and then presence of either 100 pM (light green) or 10 nM (dark green) CNO. Acute activation of the Gq pathway in *Opn4^{-/-}* M4 cells in darkness results in increases in excitability identical to those seen in WT M4 cells in background light.

All data are represented as mean \pm SEM. Recordings were made in synaptic blockers and cells were initially held at a subthreshold V_m of ~ -75 mV. Measurements were made from single cells in darkness and then in a single background light intensity or following application of CNO. ChAT, choline acetyltransferase. CNO, clozapine-N-oxide.

offset (Figure S5). These data, combined with the light-dependent increase in R_{inp} , point to a melanopsin-mediated closure of potassium leak channels in M4 cells. In support of this, when we record from M4 cells in TRPC 3/6/7 KO retinas, we find that the I-V relationship still reversed near -90 mV, though it became more linear (Figures 7C and 7D). Taken together, these data suggest that potassium leak channels are the major target of melanopsin phototransduction in M4 cells.

If the major conductance modulated by melanopsin is potassium, then increasing the extracellular potassium concentration to 18 mM should shift the reversal of the melanopsin-mediated

current to the more positive, predicted E_k of -50 mV. Indeed, under these conditions, the melanopsin-mediated current in TRPC 3/6/7 KO M4 cells reversed at the predicted E_k of -50 mV (Figure 7D), further confirming that this current is mediated by potassium channels. We then performed the same experiments in a nucleated patch configuration to mitigate any space clamp concerns (Figure 7E). In this configuration, we found that the I-V relationship of the photocurrent in nucleated M4 cells from TRPC 3/6/7 KO retinas was identical to that of intact cells (Figures 7E and 7F). These experiments further demonstrate that the major melanopsin-mediated current in M4 cells is carried by potassium.

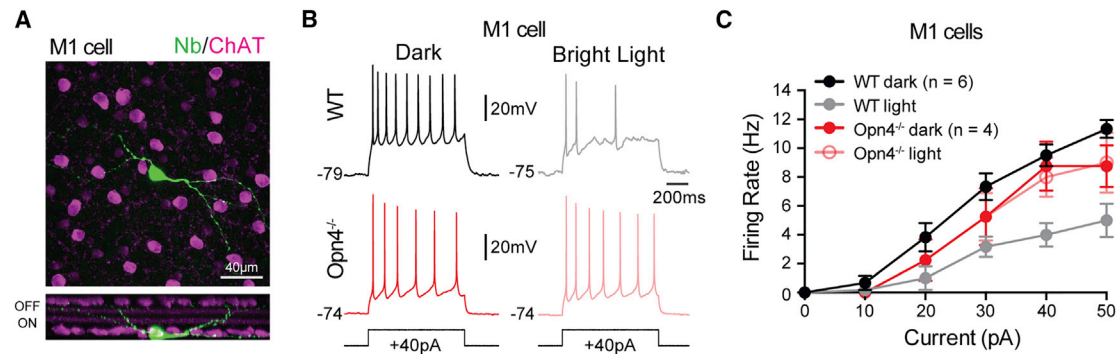


Figure 6. Melanopsin Phototransduction Decreases the Intrinsic Excitability of M1 Cells

(A) Z stack, confocal image of an M1 cell filled with Neurobiotin (Nb, green) in retina co-immunolabeled for ChAT (magenta). Bottom panel shows a Z-projected view of the same cell in the orthogonal plane.

(B) Whole-cell recording of M1 cells in response to a 40 pA current injection in WT (top panels) or *Opn4*^{-/-} (bottom panels) retinas in darkness (left panels) or 12 log quanta/cm²/s background light (right panels). Recordings were made in synaptic blockers. Cells were held at a subthreshold membrane potential of ~-75 mV prior to applying current steps. Recordings were made from single cells in darkness and then in a single background light intensity.

(C) Firing rate plotted as a function of current injected in WT M1 cells in dark (black) or 12 log quanta/cm²/s (gray) background light and *Opn4*^{-/-} M1 cells in dark (dark red) or 12 log quanta/cm²/s (light red) background light. WT cells showed a melanopsin-dependent decrease in firing to identical current injections in background light compared to darkness.

All data are represented as mean ± SEM. ChAT, choline acetyltransferase.

In order to account for the possibility that current amplitude measured at different voltages in individual cells could reflect cell to cell variability, we performed a set of experiments where we first held a cell at a test voltage from -110 mV to 0 mV, exposed the cell to 100 ms of bright (10¹² quanta/cm²/s) light in the presence of synaptic blockers and TTX, and then recorded the melanopsin photocurrent (*I*_{test}) (Figure S6A). After allowing the cell to return to baseline (5–7 min), we then held the cell at a control voltage of -80 mV and recorded the melanopsin photocurrent *I*_{control} in response to the same 100 ms stimulus, which served for normalization (Figure S6A). We found that the latency to maximum was identical across holding potentials (Figure S6D) and that the I-V relationship of both the raw *I*_{test} and of the normalized photocurrents showed a negative slope and reversed near *E*_k (Figures S6B and S6C). These data indicate that I-V relationships reported here are not a reflection of inter-cellular variability.

We next wanted to determine the pharmacological properties of the potassium leak channels closed by melanopsin. To do this, we recorded from M4 cells in TRPC 3/6/7 KO retinas in order to isolate the potassium current modulated by melanopsin phototransduction. Because the I-V relationship of the current was linear in the voltage ranges tested, we ruled out voltage-gated potassium channels and inward rectifying potassium channels (*K*_{ir}). We reasoned that the most likely candidates were the two-pore domain (K2P) family of potassium channels, which are known to be modulated by the Gq pathway and important for modulating cellular excitability (Chemin et al., 2003; Mathie, 2007; Talley et al., 2000). K2P channels are insensitive to extracellular application of the broad spectrum potassium channel blocker tetraethylammonium (TEA) (Patel and Honoré, 2001). Consistent with modulation of K2P channels, when we bath applied 1 mM TEA, we found that intrinsic light response of nucleated M4 cells was unaffected (Figures 7G and 7H).

K2P channels are composed of six subfamilies and only two of these subfamilies (TASK and TREK) are inhibited by the Gq pathway (Mathie, 2007). We therefore performed pharmacological manipulations to exploit differences in the pharmacological properties of TASK and TREK channels to identify which was the most likely target of melanopsin phototransduction. Under physiological K⁺ concentrations, TASK channels can be blocked by millimolar concentrations of extracellular Ba²⁺, while TREK channels are relatively resistant (Patel and Honoré, 2001). When we bath applied 2 mM Ba²⁺, the intrinsic light response of nucleated M4 cells was abolished (Figures 7G and 7H), consistent with the properties of TASK K2P channels. Additionally, arachidonic acid and chloroform have been reported to strongly activate TREK channels but weakly inhibit or have no effect on TASK channels (Kim, 2005; Lesage, 2003; Lotshaw, 2007). Again consistent with the properties of TASK channels, bath application of 10 μM arachidonic acid or 5 mM chloroform had no effect on the melanopsin-mediated current or holding current of M4 cells (Figures S7A–S7D). Bath application of the selective TASK 1/3 channel blocker ML 365 (Zou et al., 2010) resulted in significant increases in holding current and significant decreases in the melanopsin-mediated current (Figures S7E and S7F). Taken together, these data suggest that melanopsin phototransduction targets the TASK subfamily of K2P channels in M4 cells.

Melanopsin Phototransduction Acts through Gq and PLC

Our data so far indicate that activation of the Gq cascade through Gq-DREADDs in *Opn4*^{-/-} M4 cells is sufficient to recapitulate melanopsin-dependent effects on cellular contrast sensitivity, membrane depolarization, and intrinsic excitability (Figures 2 and 5). To test whether Gq signaling is in fact necessary for the melanopsin-mediated light response, we recorded

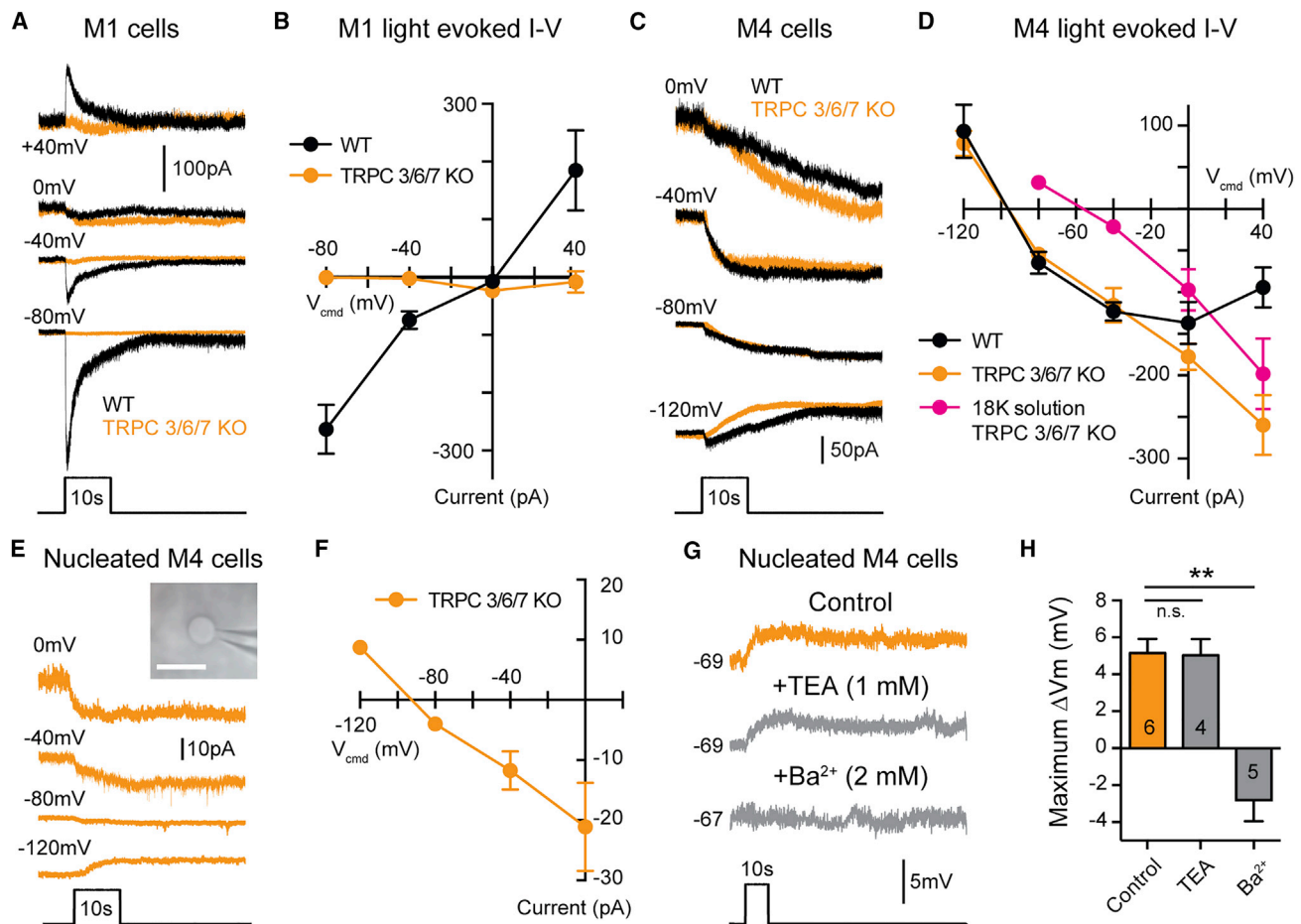


Figure 7. Leak Potassium Channels Are the Major Target of Melanopsin Phototransduction in M4 Cells

(A) Example whole-cell voltage-clamp recordings from M1 cells in WT (black) and TRPC 3/6/7 KO (orange) retinas held at multiple potentials and exposed to a 10 s light step.

(B) I-V relationship of the maximum light-evoked current recorded from M1 cells. WT M1 cell currents reverse near 0 mV ($n = 19$, 4–6 cells/group), while TRPC 3/6/7 KO M1 cell currents were almost completely abolished at all voltages tested ($n = 10$, 2–3 cells/group).

(C) Example whole-cell voltage-clamp recordings from M4 cells from WT (black) and TRPC 3/6/7 KO (orange) retinas held at multiple potentials and exposed to a 10 s light step.

(D) I-V relationship of the maximum light-evoked current recorded in M4 cells. Currents from WT M4 cells (black) exhibited a negative slope I-V relationship that reversed at approximately -90 mV ($n = 25$, 5 cells/group). Currents from TRPC 3/6/7 KO M4 cells (orange) exhibited a more linear I-V relationship that also reversed near -90 mV ($n = 23$ cells, 4–6 cells/group). In extracellular solution with 18 mM K^+ (“18K solution,” magenta), the current recorded in TRPC 3/6/7 KO M4 cells reverses near the predicted E_K of -50 mV ($n = 19$ cells, 4–5 cell/group).

(E) Example nucleated patch recordings from M4 cells in TRPC 3/6/7 KO retinas (orange). Nucleated patches were held at multiple potentials and exposed to a 10 s light step. Inset shows an example nucleated patch visualized in IR-DIC. White scale bar represents 10 μ m.

(F) I-V relationship of the maximum light-evoked current recorded from nucleated M4 cells in TRPC 3/6/7 KO retinas ($n = 16$ cells, 3–5 cells/group). The I-V relationship recorded in nucleated patch configuration closely resembles that recorded in intact cells (see panel D).

(G) Example nucleated current-clamp recording from M4 cells in TRPC 3/6/7 KO retinas exposed to a 10 s light step in control solution (L-AP4 + TTX in AMES⁺, orange) or with either 1 mM TEA or 2 mM Ba^{2+} (gray) added. Recordings in control versus drug solution were made in separate cells.

(H) Max changes in V_m of nucleated M4 cells in the presence of 1 mM extracellular TEA or 2 mM Ba^{2+} .

All data are represented as mean \pm SEM. All 10 s light steps are 12 log quanta/cm²/s. Currents for I-V relationships were measured by subtracting the baseline holding current in darkness from the maximum light-evoked current. Example traces at each voltage are from different cells. * $p < 0.05$. ** $p < 0.01$. n.s., not significant.

light-evoked currents to bright (12.5 log quanta/cm²/s) light from intact M4 cells in WT retinas in the presence of the Gq inhibitor YM-254890 (Takasaki et al., 2004). We found that the light response was completely abolished in the presence of YM-254890 (Figure S8A). We next tested whether PLC activation is

necessary for melanopsin phototransduction in M4 cells. We first performed experiments in the presence of the PLC inhibitor U73122 (Bleasdale et al., 1989). In intact M4 cells, we found that bath application of U73122 led to a significant but incomplete reduction in the melanopsin-mediated current (Figure S8B).

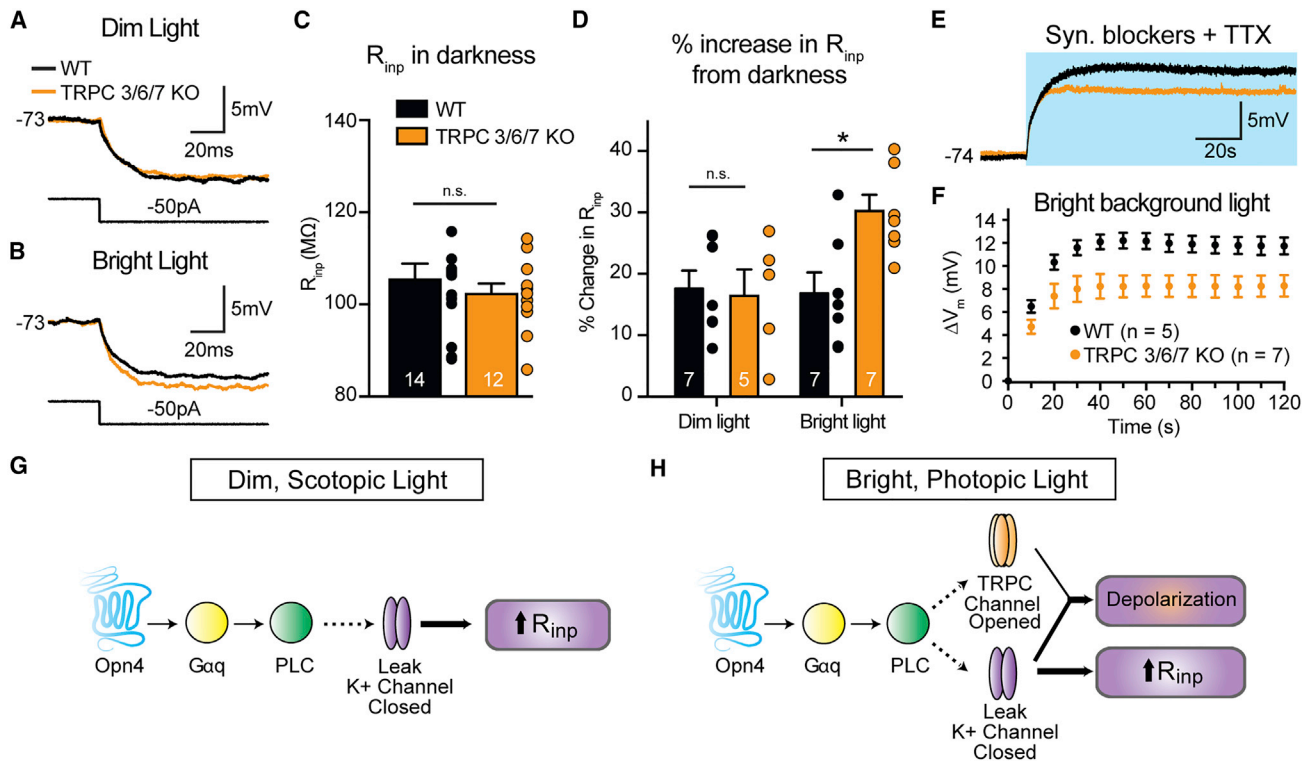


Figure 8. TRPC Channels Contribute to the Intrinsic Response of M4 Cells at Bright Light Levels

(A and B) Current-clamp recordings from intact M4 cells in WT (black) and TRPC 3/6/7 KO (orange) retinas. Traces are voltage responses to a 50 pA hyperpolarizing current injection made in dim (A, 9 log quanta/cm²/s) or bright (B, 12 log quanta/cm²/s) background light. Recordings were made in a cocktail of synaptic blockers and TTX.

(C) Input resistance (R_{in}) of intact M4 cells in WT (black) and TRPC 3/6/7 KO (orange) retinas measured in the dark. There were no significant differences in R_{in} between WT and TRPC 3/6/7 KO M4 cells in the dark.

(D) Percentage increase in R_{in} in background light from darkness. Changes in R_{in} were identical between WT (black) and TRPC 3/6/7 KO (orange) M4 cells in dim background light. In bright background light, TRPC 3/6/7 KO M4 cells exhibited larger increases in R_{in} compared to WT M4 cells.

(E) Voltage responses of intact M4 cells in WT (black) or TRPC 3/6/7 KO (orange) retinas to a 2 min bright background light stimulus of 12 log quanta/cm²/s. Blue background indicates the light stimulus.

(F) Change in membrane potential (ΔV_m) from baseline in 10 s bins over 2 min exposure to a bright background light stimulus (12 log quanta/cm²/s).

(G and H) Schematic describing melanopsin phototransduction in M4 cells at dim (scotopic, G) and bright (photopic, H) light levels. In both dim and bright light, melanopsin activates a Gq/PLC-based transduction cascade. In dim light, melanopsin phototransduction closes leak potassium channels, resulting in an increase in R_{in} . In bright light, melanopsin phototransduction closes leak potassium channels and opens TRPC channels, resulting in net depolarization of V_m and increase in R_{in} .

All data are represented as mean \pm SEM. * $p < 0.05$. n.s., not significant.

Because U73122 has previously been reported to show incomplete blockade of phototransduction in intact M1 cells (Graham et al., 2008), we next performed current-clamp recordings of nucleated patches from WT M4 cells. In this configuration, we observed a complete blockade of the melanopsin-dependent light response in the presence of the PLC inhibitor U73122 (Figure S8C). These data indicate that melanopsin phototransduction acts through a Gq-coupled pathway to activate PLC, similar to the initial steps of the transduction cascade described in M1 cells (Graham et al., 2008; Xue et al., 2011).

TRPC Channels Contribute to M4 Cell Depolarization at Bright Light Intensities

While the maximum light-evoked current of M4 cells was largely unchanged in TRPC 3/6/7 KO retinas (Figures 7C and 7D), the

more linear I-V relationship of M4 cells in these retinas points to a minor role for TRPC channels in the M4 cell light response. We therefore wanted to test directly whether TRPC channels contributed to the M4 cell light response at dim (9 log quanta/cm²/s) and bright (12 log quanta/cm²/s) light intensities. Because we could not detect a melanopsin-dependent depolarization to dim light in intact M4 cells (Figure 4), we first chose to measure melanopsin-dependent changes in R_{in} in M4 cells in dim background light in WT versus TRPC 3/6/7 KO retinas in the presence of synaptic blockers and TTX. Both WT and TRPC 3/6/7 KO M4 cells showed similar R_{in} in darkness, as well as an identical increase in R_{in} in dim background light, which suggests that TRPC channels do not open in dim light (Figures 8A–8D). Interestingly, TRPC 3/6/7 KO M4 cells showed a significantly larger increase in R_{in} in bright background light compared to

WT (Figures 8A–8D). These data suggest that TRPC channels open in response to melanopsin phototransduction only at brighter light intensities and offset the additional potassium channel closure and increases in R_{inp} that might be expected with more melanopsin activation. The identical R_{inp} in bright and dim background light in WT M4 cells likely accounts for the identical melanopsin-dependent changes in excitability observed across light levels from 9–12 log quanta/cm²/s (Figures 5B and 5C).

Based on the contribution of TRPC 3/6/7 channels to setting R_{inp} in bright light, we would predict that TRPC 3/6/7 channels enhance the melanopsin-dependent depolarization of M4 cells in response to bright light. In support of our prediction, we find that TRPC 3/6/7 KO M4 cells show a small but consistent decrease in light-evoked depolarization to 2 min of bright light compared to WT (Figures 8E and 8F). These data demonstrate that TRPC 3/6/7 channels make a minor contribution to setting R_{inp} and enhancing melanopsin-dependent depolarization at brighter light levels.

Melanopsin-Dependent Increases in R_{inp} Are Enhanced in Bright Light when Rod/Cone Inputs Are Intact

Our initial measurements of melanopsin-dependent increases in R_{inp} were made in the absence of rod and cone input. We therefore next asked whether these melanopsin-dependent increases in R_{inp} were detectable in the presence of functional rod and cone input. To test this, we measured the R_{inp} of M4 cells in dim and bright background light with synaptic blockers omitted from the extracellular solution. We found that both dim and bright background light significantly increased the R_{inp} of WT compared to *Opn4*^{-/-} M4 cells (Figures S9A and S9B). Therefore, melanopsin phototransduction is capable of producing measurable increases in R_{inp} in M4 cells when synaptic input is intact, which could significantly enhance their ability to respond to small synaptic inputs at low contrast. Moreover, in WT M4 cells, we observed significantly larger increases in R_{inp} in bright background light (~30%) compared to dim background light (~15%), which is consistent with the larger deficits in C_{50} and contrast gain of *Opn4*^{-/-} M4 cells in bright versus dim background light (Figures 1B and 1C).

DISCUSSION

The present results challenge two widely held assumptions in the field: (1) that the melanopsin phototransduction cascade acts through identical mechanisms in different ipRGC subtypes and (2) that the properties of melanopsin phototransduction in image-forming ipRGC subtypes preclude a physiologically relevant role in vision. Our data demonstrate a crucial role for melanopsin in modulating visual processing in the retina and show that melanopsin acts through distinct pathways in ipRGC subtypes to exert profound influences on the visual signals relayed for image and non-image forming behaviors. In particular, our results point to melanopsin as a major intracellular modulator of how rod and cone signals are processed.

Melanopsin Acts through a Novel Transduction Channel in M4 Cells

Melanopsin phototransduction has been reported to activate a Gq cascade that results in the opening of TRPC 6/7 channels

in M1 cells (Graham et al., 2008; Hartwick et al., 2007; Perez-Leighton et al., 2011; Warren et al., 2006; Xue et al., 2011). Though melanopsin phototransduction has been primarily examined in M1 cells and heterologous systems, it has been widely assumed that the melanopsin phototransduction cascade would activate similar downstream targets in all ipRGC subtypes. This assumption was rooted in the observation that melanopsin phototransduction in M1 cells resembled rhabdomic phototransduction cascades (Graham et al., 2008; Melyan et al., 2005; Panda et al., 2005; Perez-Leighton et al., 2011; Qiu et al., 2005; Xue et al., 2011), which are highly conserved and couple to the Gq class of G-proteins, activate PLC, and open TRPC channels (Berson, 2007; Hardie and Raghu, 2001; Lamb, 2013; Plachetzki et al., 2010). Melanopsin phototransduction also elicits depolarizing responses in all other ipRGC subtypes, consistent with opening of TRPC channels (Schmidt and Kofuji, 2009; Ecker et al., 2010; Estevez et al., 2012; Hu et al., 2013; Zhao et al., 2014). Our data indicate that the initial steps of the melanopsin phototransduction cascade in M4 cells are similar to those reported previously, with activation of Gq and PLC by melanopsin (Figures 8G and 8H).

Our results demonstrate that melanopsin phototransduction results in a closure of potassium leak channels in M4 cells, which represent a novel target of the melanopsin transduction cascade (Figures 8G and 8H). The melanopsin-dependent decrease in potassium conductance and resulting increase in excitability in M4 cells is consistent with previous reports in non-retinal tissues that closure of potassium channels by the Gq pathway increases cellular excitability (Bista et al., 2015; Peters et al., 2005; Soh et al., 2014). Our data are consistent with modulation of K2P channels because the melanopsin-mediated current in M4 cells exhibits a linear I-V relationship and we observed a melanopsin-dependent increase in R_{inp} in background light. Additionally, we find that the melanopsin-mediated current in M4 cells is TEA insensitive, which is also broadly consistent with the pharmacological properties of K2P channels (Kim, 2005; Patel and Honoré, 2001). The sensitivity to extracellular Ba²⁺ and ML 365 and insensitivity to arachidonic acid and chloroform is consistent with a specific modulation of the TASK subfamily of K2P channels, which is one of two K2P subfamilies that are closed by Gq activation (Mathie 2007). TASK K2P channels have previously been shown to be expressed in the ganglion cell layer of the retina, which combined with our pharmacological data, makes them a likely candidate for melanopsin modulation (Hughes et al., 2017).

Melanopsin Enhances the Visual Signaling of an Image-Forming ipRGC Subtype

M4 cells are synonymous with ON alpha RGCs, which are known to be highly sensitive to contrast (Grimes et al., 2014; Schmidt et al., 2014; Zaghoul et al., 2003). Our results demonstrate that melanopsin phototransduction is a critical component of this defining feature of ON alpha RGCs and points to these cells as a major relay of melanopsin signals to downstream visual areas. Moreover, melanopsin phototransduction enhances the contrast sensitivity of M4 cells across a wide range of commonly encountered environmental light levels ranging from dim, scotopic intensities where only rod phototransduction was thought to be active, to bright, photopic light intensities

where cone phototransduction predominates. Therefore, our results indicate that melanopsin's potential to modulate visual processing extends across a much wider, and more physiological, range of light intensities than previously appreciated.

Our data provide a model by which melanopsin phototransduction could influence cellular contrast sensitivity at dim and bright light levels (Figures 8G, 8H, and S9C). In dim light, closure of potassium leak channels increases R_{inp} , which leads to an increase in intrinsic excitability. Our data also show that in dim background light, melanopsin phototransduction does not directly depolarize intact M4 cells, though we can detect melanopsin-mediated depolarization at this light intensity in the nucleated patch configuration (Figure 4). However, melanopsin phototransduction serves to maintain the V_m of M4 cells near that in darkness and above that seen in *Opn4*^{-/-} M4 cells when rod and cone pathways are intact (Figures 3 and S2). This is significant because type 6 ON cone bipolar cells, which are the dominant excitatory input onto M4 cells, hyperpolarize in tonic dim background light relative to baseline V_m in darkness (Grimes et al., 2014). Therefore, if melanopsin had no effect on M4 cell V_m in dim light, we would expect these cells to also hyperpolarize like the presynaptic type 6 bipolar cells, which is consistent with our observations in *Opn4*^{-/-} M4 cells (Figures 3 and S2). It is also possible that melanopsin does not directly depolarize V_m of M4 cells in dim light when synaptic blockers are present because the cell rests at a hyperpolarized V_m where the driving force for potassium would be low (Figure 4). However, with rod/cone inputs intact, M4 cells rest at a more depolarized V_m , making it possible that melanopsin phototransduction (perhaps in conjunction with rod/cone inputs) does contribute to the depolarized V_m of M4 cells in dim light (Figure 3). These data suggest that melanopsin-mediated increases in R_{inp} in dim background light amplify the tonic synaptic input from cone bipolar cells, which prevents M4 cells from hyperpolarizing relative to their dark V_m . Thus, by maintaining V_m near spike threshold and increasing R_{inp} , melanopsin phototransduction enhances the small inputs relayed from rods under dim, scotopic conditions, thereby enhancing the contrast sensitivity of the cell (Figure S9).

In bright background light, melanopsin phototransduction directly depolarizes M4 cell resting V_m in addition to increasing R_{inp} and intrinsic excitability. TRPC channels are also opened at brighter light levels and contribute to a small enhancement of V_m depolarization (Figures 8A–8F). By maintaining V_m closer to/further above spike threshold and increasing R_{inp} , melanopsin phototransduction serves to increase the probability that a given signal relayed from rod/cone photoreceptors will elicit a change in firing frequency in the M4 cell and be relayed to the brain. This would be particularly important near contrast threshold, where the signals relayed from the rods or cones would be smallest. The closure of potassium channels as the major source of depolarizing current is significant because exclusively opening TRPC channels would similarly depolarize V_m but would also lead to a counterproductive decrease in R_{inp} . Thus, the closure of potassium leak channels serves the added function of amplifying the response of M4 cells to rod and cone inputs, thereby enhancing contrast sensitivity. The fact that melanopsin-mediated changes in intrinsic excitability are identical across light intensities and

perfectly offset by a TRPC conductance demonstrates the precise tuning of this response for proper M4 cell function (Figures 4 and 8). This simultaneous decrease of potassium leak conductance and increase of cationic conductance to increase cellular excitability is a well-documented effect of neuromodulators in other systems (Fisher and Nistri, 1993; Hsiao et al., 1997; Larkman and Kelly, 1992; Shen and Surprenant, 1993). Thus, while it is useful to study melanopsin phototransduction or rod and cone inputs to ipRGCs in isolation, there are important interactions between these systems that are required to modulate the visual responses of ipRGCs that will ultimately be relayed to the brain.

In summary, our data clearly show that melanopsin drives distinct conductance changes in ipRGC subtypes specialized for different visual functions. These divergent physiological influences of melanopsin on ipRGCs specialized for image-forming (M4 cell) versus non-image forming (M1 cell) visual behaviors serve to tune cellular function for the specific functions of each subtype.

STAR★METHODS

Detailed methods are provided in the online version of this paper and include the following:

- KEY RESOURCES TABLE
- CONTACT FOR REAGENT AND RESOURCE SHARING
- EXPERIMENTAL MODEL AND SUBJECT DETAILS
- METHOD DETAILS
 - *Ex vivo* Retina Preparation for Electrophysiology
 - Solutions for Electrophysiology
 - Visual Stimuli
 - Electrophysiology
 - Viral Infection
 - Immunohistochemistry
- QUANTIFICATION AND STATISTICAL ANALYSIS
- DATA AND SOFTWARE AVAILABILITY

SUPPLEMENTAL INFORMATION

Supplemental Information includes nine figures and can be found with this article online at <https://doi.org/10.1016/j.neuron.2018.06.032>.

ACKNOWLEDGMENTS

We would like to thank Marco Gallio, Indira Raman, Jianhua Cang, Gregory Schwartz, Paulo Kofuji, Samer Hattar, Marnie Halpern, and Thomas Bozza for helpful comments on the manuscript. We would like to thank Yin-Peng Chen for scientific illustrations, Samer Hattar for the gift of the *Opn4*^{LacZ} and *Opn4*^{Cre} lines, and Marla Feller for the gift of the *Opn4*-GFP line. This work was funded by a Karl Kirchgessner Foundation Vision Research Grant to T.M.S., a Klingenstein-Simons Fellowship in the Neurosciences to T.M.S., NIH grant 1DP2EY022584 to T.M.S., NIH T32 EY025202 to support T.S., and the Intramural Research Program of the NIH (Project Z01-ES-101684 to L.B.).

AUTHOR CONTRIBUTIONS

T.S. and T.M.S. designed the experiments, wrote the paper, and prepared the figures. T.S. collected data for all experiments and S.K.L. helped with imaging as well as data collection for M1 cell experiments. T.S. analyzed the data. L.B. generated the TRPC 3/6/7 knockout animals.

DECLARATION OF INTERESTS

The authors declare no competing interests.

Received: June 27, 2017

Revised: January 7, 2018

Accepted: June 20, 2018

Published: July 12, 2018

REFERENCES

- Albrecht, D.G., and Hamilton, D.B. (1982). Striate cortex of monkey and cat: contrast response function. *J. Neurophysiol.* **48**, 217–237.
- Berson, D.M. (2007). Phototransduction in ganglion-cell photoreceptors. *Pflugers Arch.* **454**, 849–855.
- Berson, D.M., Dunn, F.A., and Takao, M. (2002). Phototransduction by retinal ganglion cells that set the circadian clock. *Science* **295**, 1070–1073.
- Bista, P., Pawlowski, M., Cerina, M., Ehling, P., Leist, M., Meuth, P., Aissaoui, A., Borsotto, M., Heurteaux, C., Decher, N., et al. (2015). Differential phospholipase C-dependent modulation of TASK and TREK two-pore domain K⁺ channels in rat thalamocortical relay neurons. *J. Physiol.* **593**, 127–144.
- Bleasdale, J.E., Bundy, G.L., Bunting, S., Fitzpatrick, F.A., Huff, R.M., Sun, F.F., and Pike, J.E. (1989). Inhibition of phospholipase C dependent processes by U-73, 122. *Adv. Prostaglandin Thromboxane Leukot. Res.* **19**, 590–593.
- Brainard, D.H. (1997). The Psychophysics Toolbox. *Spat. Vis.* **10**, 433–436.
- Brown, D.A., and Passmore, G.M. (2009). Neural KCNQ (Kv7) channels. *Br. J. Pharmacol.* **156**, 1185–1195.
- Chemin, J., Girard, C., Duprat, F., Lesage, F., Romey, G., and Lazdunski, M. (2003). Mechanisms underlying excitatory effects of group I metabotropic glutamate receptors via inhibition of 2P domain K⁺ channels. *EMBO J.* **22**, 5403–5411.
- Dietrich, A., Mederos Y Schnitzler, M., Gollasch, M., Gross, V., Storch, U., Dubrovskaya, G., Obst, M., Yildirim, E., Salanova, B., Kalwa, H., et al. (2005). Increased vascular smooth muscle contractility in TRPC6^{-/-} mice. *Mol. Cell Biol.* **25**, 6980–6989.
- Do, M.T., and Yau, K.-W.W. (2013). Adaptation to steady light by intrinsically photosensitive retinal ganglion cells. *Proc. Natl. Acad. Sci. USA* **110**, 7470–7475.
- Ecker, J.L., Dumitrescu, O.N., Wong, K.Y., Alam, N.M., Chen, S.-K.K., LeGates, T., Renna, J.M., Prusky, G.T., Berson, D.M., and Hattar, S. (2010). Melanopsin-expressing retinal ganglion-cell photoreceptors: cellular diversity and role in pattern vision. *Neuron* **67**, 49–60.
- Emanuel, A.J., Kapur, K., and Do, M.T.H. (2017). Biophysical Variation within the M1 Type of Ganglion Cell Photoreceptor. *Cell Rep.* **21**, 1048–1062.
- Estevez, M.E., Fogerson, P.M., Ilardi, M.C., Borghuis, B.G., Chan, E., Weng, S., Auferkorte, O.N., Demb, J.B., and Berson, D.M. (2012). Form and function of the M4 cell, an intrinsically photosensitive retinal ganglion cell type contributing to geniculocortical vision. *J. Neurosci.* **32**, 13608–13620.
- Feliciangeli, S., Chatelain, F.C., Bichet, D., and Lesage, F. (2015). The family of K2P channels: salient structural and functional properties. *J. Physiol.* **593**, 2587–2603.
- Fisher, N.D., and Nistri, A. (1993). A study of the barium-sensitive and -insensitive components of the action of thyrotropin-releasing hormone on lumbar motoneurons of the rat isolated spinal cord. *Eur. J. Neurosci.* **5**, 1360–1369.
- Graham, D.M., Wong, K.Y., Shapiro, P., Frederick, C., Pattabiraman, K., and Berson, D.M. (2008). Melanopsin ganglion cells use a membrane-associated rhabdomic phototransduction cascade. *J. Neurophysiol.* **99**, 2522–2532.
- Greene, D.L., and Hoshi, N. (2017). Modulation of Kv7 channels and excitability in the brain. *Cell. Mol. Life Sci.* **74**, 495–508.
- Grimes, W.N., Schwartz, G.W., and Rieke, F. (2014). The synaptic and circuit mechanisms underlying a change in spatial encoding in the retina. *Neuron* **82**, 460–473.
- Grubb, M.S., and Thompson, I.D. (2003). Quantitative characterization of visual response properties in the mouse dorsal lateral geniculate nucleus. *J. Neurophysiol.* **90**, 3594–3607.
- Güler, A.D., Ecker, J.L., Lall, G.S., Haq, S., Altimus, C.M., Liao, H.-W.W., Barnard, A.R., Cahill, H., Badea, T.C., Zhao, H., et al. (2008). Melanopsin cells are the principal conduits for rod-cone input to non-image-forming vision. *Nature* **453**, 102–105.
- Hardie, R.C., and Raghu, P. (2001). Visual transduction in *Drosophila*. *Nature* **413**, 186–193.
- Hartmann, J., Dragicevic, E., Adelsberger, H., Henning, H.A., Sumser, M., Abramowitz, J., Blum, R., Dietrich, A., Freichel, M., Flockerzi, V., et al. (2008). TRPC3 channels are required for synaptic transmission and motor coordination. *Neuron* **59**, 392–398.
- Hartwick, A.T., Bramley, J.R., Yu, J., Stevens, K.T., Allen, C.N., Baldrige, W.H., Sollars, P.J., and Pickard, G.E. (2007). Light-evoked calcium responses of isolated melanopsin-expressing retinal ganglion cells. *J. Neurosci.* **27**, 13468–13480.
- Hatori, M., Le, H., Vollmers, C., Keding, S.R., Tanaka, N., Buch, T., Waisman, A., Schmedt, C., Jegla, T., and Panda, S. (2008). Inducible ablation of melanopsin-expressing retinal ganglion cells reveals their central role in non-image forming visual responses. *PLoS ONE* **3**, e2451.
- Hattar, S., Liao, H.W., Takao, M., Berson, D.M., and Yau, K.W. (2002). Melanopsin-containing retinal ganglion cells: architecture, projections, and intrinsic photosensitivity. *Science* **295**, 1065–1070.
- Hsiao, C.F., Trueblood, P.R., Levine, M.S., and Chandler, S.H. (1997). Multiple effects of serotonin on membrane properties of trigeminal motoneurons in vitro. *J. Neurophysiol.* **77**, 2910–2924.
- Hu, C., Hill, D.D., and Wong, K.Y. (2013). Intrinsic physiological properties of the five types of mouse ganglion-cell photoreceptors. *J. Neurophysiol.* **109**, 1876–1889.
- Hughes, S., Foster, R.G., Peirson, S.N., and Hankins, M.W. (2017). Expression and localisation of two-pore domain (K2P) background leak potassium ion channels in the mouse retina. *Sci. Rep.* **7**, 46085.
- Kim, D. (2005). Physiology and pharmacology of two-pore domain potassium channels. *Curr. Pharm. Des.* **11**, 2717–2736.
- Krashes, M.J., Koda, S., Ye, C., Rogan, S.C., Adams, A.C., Cusher, D.S., Maratos-Flier, E., Roth, B.L., and Lowell, B.B. (2011). Rapid, reversible activation of AgRP neurons drives feeding behavior in mice. *J. Clin. Invest.* **121**, 1424–1428.
- Laboissonniere, L.A., Sonoda, T., Lee, S.K., Trimarchi, J.M., and Schmidt, T.M. (2017). Single-cell RNA-Seq of Defined Subsets of Retinal Ganglion Cells. *J. Vis. Exp.* (123).
- Lamb, T.D. (2013). Evolution of phototransduction, vertebrate photoreceptors and retina. *Prog. Retin. Eye Res.* **36**, 52–119.
- Larkman, P.M., and Kelly, J.S. (1992). Ionic mechanisms mediating 5-hydroxytryptamine- and noradrenaline-evoked depolarization of adult rat facial motoneurons. *J. Physiol.* **456**, 473–490.
- Lesage, F. (2003). Pharmacology of neuronal background potassium channels. *Neuropharmacology* **44**, 1–7.
- Lotshaw, D.P. (2007). Biophysical, pharmacological, and functional characteristics of cloned and native mammalian two-pore domain K⁺ channels. *Cell Biochem. Biophys.* **47**, 209–256.
- Lucas, R.J., Hattar, S., Takao, M., Berson, D.M., Foster, R.G., and Yau, K.-W.W. (2003). Diminished pupillary light reflex at high irradiances in melanopsin-knockout mice. *Science* **299**, 245–247.
- Mathie, A. (2007). Neuronal two-pore-domain potassium channels and their regulation by G protein-coupled receptors. *J. Physiol.* **578**, 377–385.
- Melyan, Z., Tartelin, E.E., Bellingham, J., Lucas, R.J., and Hankins, M.W. (2005). Addition of human melanopsin renders mammalian cells photoresponsive. *Nature* **433**, 741–745.
- Milner, E.S., and Do, M.T.H. (2017). A Population Representation of Absolute Light Intensity in the Mammalian Retina. *Cell* **171**, 865–876.e16.

- O'Brien, B.J., Isayama, T., Richardson, R., and Berson, D.M. (2002). Intrinsic physiological properties of cat retinal ganglion cells. *J. Physiol.* 538, 787–802.
- Panda, S., Nayak, S.K., Campo, B., Walker, J.R., Hogenesch, J.B., and Jegla, T. (2005). Illumination of the melanopsin signaling pathway. *Science* 307, 600–604.
- Pang, J.-J., Gao, F., and Wu, S.M. (2003). Light-evoked excitatory and inhibitory synaptic inputs to ON and OFF alpha ganglion cells in the mouse retina. *J. Neurosci.* 23, 6063–6073.
- Patel, A.J., and Honoré, E. (2001). Properties and modulation of mammalian 2P domain K⁺ channels. *Trends Neurosci.* 24, 339–346.
- Perez-Leighton, C.E., Schmidt, T.M., Abramowitz, J., Birnbaumer, L., and Kofuji, P. (2011). Intrinsic phototransduction persists in melanopsin-expressing ganglion cells lacking diacylglycerol-sensitive TRPC subunits. *Eur. J. Neurosci.* 33, 856–867.
- Peters, H.C., Hu, H., Pongs, O., Storm, J.F., and Isbrandt, D. (2005). Conditional transgenic suppression of M channels in mouse brain reveals functions in neuronal excitability, resonance and behavior. *Nat. Neurosci.* 8, 51–60.
- Plachetzki, D.C., Fong, C.R., and Oakley, T.H. (2010). The evolution of phototransduction from an ancestral cyclic nucleotide gated pathway. *Proc. Biol. Sci.* 277, 1963–1969.
- Prusky, G.T., and Douglas, R.M. (2004). Characterization of mouse cortical spatial vision. *Vision Res.* 44, 3411–3418.
- Qiu, X., Kumbalaliri, T., Carlson, S.M., Wong, K.Y., Krishna, V., Provencio, I., and Berson, D.M. (2005). Induction of photosensitivity by heterologous expression of melanopsin. *Nature* 433, 745–749.
- Rao, S., Chun, C., Fan, J., Kofron, J.M., Yang, M.B., Hegde, R.S., Ferrara, N., Copenhagen, D.R., and Lang, R.A. (2013). A direct and melanopsin-dependent fetal light response regulates mouse eye development. *Nature* 494, 243–246.
- Ruby, N.F., Brennan, T.J., Xie, X., Cao, V., Franken, P., Heller, H.C., and O'Hara, B.F. (2002). Role of melanopsin in circadian responses to light. *Science* 298, 2211–2213.
- Sarnaik, R., Chen, H., Liu, X., and Cang, J. (2014). Genetic disruption of the On visual pathway affects cortical orientation selectivity and contrast sensitivity in mice. *J. Neurophysiol.* 111, 2276–2286.
- Schmidt, T.M., and Kofuji, P. (2009). Functional and morphological differences among intrinsically photosensitive retinal ganglion cells. *J. Neurosci.* 29, 476–482.
- Schmidt, T.M., and Kofuji, P. (2010). Differential cone pathway influence on intrinsically photosensitive retinal ganglion cell subtypes. *J. Neurosci.* 30, 16262–16271.
- Schmidt, T.M., and Kofuji, P. (2011). Structure and function of bistratified intrinsically photosensitive retinal ganglion cells in the mouse. *J. Comp. Neurol.* 519, 1492–1504.
- Schmidt, T.M., Taniguchi, K., and Kofuji, P. (2008). Intrinsic and extrinsic light responses in melanopsin-expressing ganglion cells during mouse development. *J. Neurophysiol.* 100, 371–384.
- Schmidt, T.M., Chen, S.-K.K., and Hattar, S. (2011). Intrinsically photosensitive retinal ganglion cells: many subtypes, diverse functions. *Trends Neurosci.* 34, 572–580.
- Schmidt, T.M., Alam, N.M., Chen, S., Kofuji, P., Li, W., Prusky, G.T., and Hattar, S. (2014). A role for melanopsin in alpha retinal ganglion cells and contrast detection. *Neuron* 82, 781–788.
- Shen, K.Z., and Surprenant, A. (1993). Common ionic mechanisms of excitation by substance P and other transmitters in guinea-pig submucosal neurons. *J. Physiol.* 462, 483–501.
- Soh, H., Pant, R., LoTurco, J.J., and Tzingounis, A.V. (2014). Conditional deletions of epilepsy-associated KCNQ2 and KCNQ3 channels from cerebral cortex cause differential effects on neuronal excitability. *J. Neurosci.* 34, 5311–5321.
- Sonoda, T., and Schmidt, T.M. (2016). Re-evaluating the Role of Intrinsically Photosensitive Retinal Ganglion Cells: New Roles in Image-Forming Functions. *Integr. Comp. Biol.* 56, 834–841.
- Stabio, M.E., Sabbah, S., Quattrochi, L.E., Ilardi, M.C., Fogerson, P.M., Leyrer, M.L., Kim, M.T., Kim, I., Schiel, M., Renna, J.M., et al. (2018). The M5 Cell: A Color-Opponent Intrinsically Photosensitive Retinal Ganglion Cell. *Neuron* 97, 150–163.e4.
- Takasaki, J., Saito, T., Taniguchi, M., Kawasaki, T., Moritani, Y., Hayashi, K., and Kobori, M. (2004). A novel Galphaq/11-selective inhibitor. *J. Biol. Chem.* 279, 47438–47445.
- Talley, E.M., Lei, Q., Sirois, J.E., and Bayliss, D.A. (2000). TASK-1, a two-pore domain K⁺ channel, is modulated by multiple neurotransmitters in motoneurons. *Neuron* 25, 399–410.
- Warren, E.J., Allen, C.N., Brown, R.L., and Robinson, D.W. (2003). Intrinsic light responses of retinal ganglion cells projecting to the circadian system. *Eur. J. Neurosci.* 17, 1727–1735.
- Warren, E.J., Allen, C.N., Brown, R.L., and Robinson, D.W. (2006). The light-activated signaling pathway in SCN-projecting rat retinal ganglion cells. *Eur. J. Neurosci.* 23, 2477–2487.
- Wong, K.Y. (2012). A retinal ganglion cell that can signal irradiance continuously for 10 hours. *J. Neurosci.* 32, 11478–11485.
- Wong, K.Y., Dunn, F.A., Graham, D.M., and Berson, D.M. (2007). Synaptic influences on rat ganglion-cell photoreceptors. *J. Physiol.* 582, 279–296.
- Xue, T., Do, M.T., Riccio, A., Jiang, Z., Hsieh, J., Wang, H.C., Merbs, S.L., Welsbie, D.S., Yoshioka, T., Weissgerber, P., et al. (2011). Melanopsin signaling in mammalian iris and retina. *Nature* 479, 67–73.
- Zaghloul, K.A., Boehn, K., and Demb, J.B. (2003). Different circuits for ON and OFF retinal ganglion cells cause different contrast sensitivities. *J. Neurosci.* 23, 2645–2654.
- Zhao, X., Stafford, B.K., Godin, A.L., King, W.M., and Wong, K.Y. (2014). Photoresponse diversity among the five types of intrinsically photosensitive retinal ganglion cells. *J. Physiol.* 592, 1619–1636.
- Zou, B., Flaherty, D.P., Simpson, D.S., Maki, B.E., Miller, M.R., Shi, J., Wu, M., McManus, O.B., Golden, J.E., Aubé, J., et al. (2010). ML365: Development of bis-amides as selective inhibitors of the KCNK3/TASK1 two pore potassium channel. Probe Reports from the NIH Molecular Libraries Program (National Center for Biotechnology Information).

STAR★METHODS

KEY RESOURCES TABLE

REAGENT or RESOURCE	SOURCE	IDENTIFIER
Antibodies		
Mouse anti-SMI-32 monoclonal antibody	BioLegend	Cat#801701; RRID: AB_509997; Lot#B237480
Goat anti-choline acetyltransferase polyclonal antibody	Millipore	Cat#AB144P; RRID: AB_090650; Lot#2558394
Alexa 546 donkey anti-goat IgG secondary antibody	ThermoFisher	Cat#A-11056; RRID: AB_2534103; Lot#1842800
Alexa 647 donkey anti-mouse IgG secondary antibody	ThermoFisher	Cat#A-31571; RRID: AB_162542; Lot#1757130
Bacterial and Virus Strains		
AAV2/hSyn-DIO-hM3D(Gq)-mCherry	UNC Vectore Core	N/A
AAV2/hSyn-DIO-hM3D(Gq)-mCherry	Addgene; Krashes et al., 2011	Addgene Cat#44361-AAV2
Chemicals, Peptides, and Recombinant Proteins		
Tetrodotoxin (TTX) Citrate	Tocris Bioscience	Cat#1069
QX-314 Chloride	Tocris Bioscience	Cat#2313
ML 365	Tocris Bioscience	Cat#5337
DNQX	Tocris Bioscience	Cat#0189
L-AP4	Tocris Bioscience	Cat#0103
Arachidonic Acid	Tocris Bioscience	Cat#2756
U 73122	Tocris Bioscience	Cat#1268
Clozapine N-Oxide (CNO)	Tocris Bioscience	Cat#4936
Tocrisolve 100	Tocris Bioscience	Cat#1684
Neurobiotin Tracer	Vector Laboratories	Cat#SP-1120-20
Picrotoxin	Sigma-Aldrich	Cat#1675
Strychnine	Sigma-Aldrich	Cat#S0532
Barium Chloride	Sigma-Aldrich	Cat#B0750
Tetraethylammonium (TEA)	Sigma-Aldrich	Cat#T2265
Chloroform	Sigma-Aldrich	Cat#C2432
YM-254890	Wako Chemicals	Cat#257-00631
Collagenase, Purified	Worthington Biochemical	Cat#LS005273
Hyaluronidase	Worthington Biochemical	Cat#LS002592
Experimental Models: Organisms/Strains		
Mouse: <i>Opn4^{LacZ/LacZ}</i>	Hattar et al., 2002	N/A
Mouse: <i>Opn4^{Cre/Cre}</i>	Ecker et al., 2010	N/A
Mouse: <i>Opn4-GFP</i> (BAC transgenic reporter)	Schmidt et al., 2008	N/A
Mouse: <i>Trpc3^{-/-}</i>	Hartmann et al., 2008	RRID: MGI:3810154
Mouse: <i>Trpc6^{-/-}</i>	Dietrich et al., 2005	RRID: MGI:3623137
Mouse: <i>Trpc7^{-/-}</i>	Perez-Leighton et al., 2011	RRID: MGI:5296035
Software and Algorithms		
MATLAB (R2015a)	MathWorks	https://www.mathworks.com/products/matlab/ ; RRID: SCR_001622
pClamp 10.7	Molecular Devices	https://www.moleculardevices.com/ ; RRID: SCR_011323
Graphpad Prism 6	GraphPad	https://www.graphpad.com/ ; RRID: SCR_002798

CONTACT FOR REAGENT AND RESOURCE SHARING

Requests for reagents and resources should be directed to the Lead Contact, Tiffany Schmidt (tiffany.schmidt@northwestern.edu).

EXPERIMENTAL MODEL AND SUBJECT DETAILS

All procedures were approved by the Animal Care and Use Committee at Northwestern University. All mice were between 1–3 months old and on a mixed B6/129 background. Both male and female mice were used. For M4 cell recordings, WT, *Opn4*^{LacZ/LacZ} (Hattar et al., 2002) and *Trpc3*^{-/-} (Hartmann et al., 2008); *Trpc6*^{-/-} (Dietrich et al., 2005); *Trpc7*^{-/-} (Perez-Leighton et al., 2011) mice were used. For Gq-DREADD rescue experiments, *Opn4*^{Cre/Cre} (Ecker et al., 2010) mice were used instead of *Opn4*^{LacZ/LacZ}. For M1 cell recordings, *Opn4*-GFP (Schmidt et al., 2008), *Opn4*^{LacZ/LacZ}; *Opn4*-GFP and *Trpc3*^{-/-}; *Trpc6*^{-/-}; *Trpc7*^{-/-}; *Opn4*-GFP mice were used.

METHOD DETAILS

Ex vivo Retina Preparation for Electrophysiology

Mice were dark-adapted overnight and sacrificed by CO₂ asphyxiation. Eyes were enucleated and retinas were dissected under dim red light in carbogenated (95% O₂-5% CO₂) Ames' medium (Sigma-Aldrich). Retinas were sliced in half and incubated in carbogenated Ames' medium at 26°C for at least 30 min prior to use. Before recording, retinas were treated with collagenase/hyaluronidase (240 and 1000 U/mL, respectively) solution in Ames' medium for 1–2 min at room temperature. Retinas were mounted on a glass-bottom recording chamber and anchored using a platinum ring with nylon mesh (Warner Instruments). The chamber was placed on an electrophysiology rig and the tissue was perfused with carbogenated Ames' medium (25–26°C, which improved the stability of recordings lasting more than 10 min and undertaken in background illumination) at 7–9 mL/min for experiments without synaptic blocker cocktail and 2–4 mL/min for experiments with synaptic blocker cocktail.

Solutions for Electrophysiology

All recordings were made in Ames' medium with 23 mM sodium bicarbonate unless noted otherwise. For extracellular loose-patch recordings, pipettes were filled with Ames' medium. For experiments with synaptic blocker cocktail, 100 μM DNQX (Tocris), 10–20 μM L-AP4 (Tocris), 50 μM picrotoxin (Sigma), 20 μM strychnine (Sigma) were added to Ames' medium. 500 nM tetrodotoxin (TTX) citrate (Tocris) was added for voltage-clamp experiments. A potassium based internal solution was used for all whole-cell recordings with the exception of experiments in which excitatory synaptic inputs were measured in Figures S1C and S1D. The potassium based internal solution contained (in mM): 125 K-gluconate, 2 CaCl₂, 2 MgCl₂, 10 EGTA, 10 HEPES, 2 Na₂-ATP, 0.5 Na-GTP, and 0.3% Neurobiotin (Vector Laboratories). The equilibrium potential of potassium (E_K) using these solutions was calculated to be -91.4 mV. For experiments measuring excitatory synaptic inputs (Figures S1C and S1D), a cesium based internal solution was used which contained (in mM): 125 Cs-methanesulfonate, 10 CsCl, 1 MgCl₂, 5 EGTA, 10 Na-HEPES, 2 Na₂-ATP, 0.5 Na-GTP, 10 Phosphocreatine, and 2 QX-314.

“18K solution” contained (in mM): 112 NaCl, 18 KCl, 1.25 NaH₂PO₃, 25 NaHCO₃, 25 Glucose, 2 CaCl₂, 1 MgCl₂. E_K using the 18K solution and the potassium based internal solution was -50 mV. QX-314 chloride (2 mM, Tocris) was added to the potassium based internal solution in experiments indicating addition of QX-314. The Gq inhibitor, YM-254890 (Wako Chemicals) was dissolved in DMSO at 10 mM and added to internal solution (1:1000) for a final concentration of 10 μM. 0.1% DMSO was added to the internal solution for the vehicle control. U73122 (Tocris) was dissolved in chloroform at 100 mM and added to the extracellular solution (1:10000) for a final concentration of 10 μM. 0.01% chloroform was added to the extracellular solution for the vehicle control. Arachidonic acid (Tocris) was purchased dissolved in Tocrisolve 100 (Tocris). Therefore, Tocrisolve 100 was added to the cocktail of synaptic blockers and TTX for the vehicle control. ML 365 (Tocris) was dissolved in DMSO at 100 mM and added to the extracellular solution for a final concentration of 20 μM. 0.2% DMSO was added to the extracellular solution for the vehicle control. Pharmacological agents were always applied for less than 5 min to minimize off-target effects.

Visual Stimuli

Visual stimuli were presented using a DLP Light Crafter 4500 projection device (Texas Instruments, refresh rate 60Hz) and images were focused onto the photoreceptor layer of *ex vivo* retinas through the microscope condenser. The blue LED (~480 nm) on the device was used and photon flux was attenuated using neutral density filters (Thor Labs). Full-field drifting sine-wave gratings were modulated at 2 cycles/second with a spatial frequency of 0.04 cycles/degree (750 μm/cycle, Figures 1A–1C) or 0.089 cycles/degree (340 μm/cycle, Figures 1D and 1E). Drifting-gratings were generated in MATLAB (Mathworks) using the Psychophysics toolbox (Brainard, 1997).

Electrophysiology

The ganglion cell layer of the retina was visualized using infrared differential interference (IR-DIC) optics at 940 nm. M4 cells were identified in IR-DIC as cells with large somata (>20 μm) and by characteristic ON-sustained responses to increments in light. Sustained-OFF alpha RGCs were identified in IR-DIC as cells with large somata and by characteristic sustained increases in firing to decrements in light (Pang et al., 2003). Alpha cell identity was confirmed after all intracellular recordings by immunolabeling cells for SMI-32. In experiments recording from Gq-DREADD infected retinas, M4 cells were visualized in epifluorescence after electrophysiological recordings to determine whether they were infected with Gq-DREADDs.

M1 cells were identified in the *Opn4-GFP* line using 2-photon excitation (910 nm). Alexa 594 hydrazide (10 μ M, Thermo) was added to the internal solution for M1 cell recordings and M1 cell identity was confirmed after recording by confirming dendrites stratified only in the OFF-sublamina of the inner plexiform layer using epifluorescence (Laboissonniere et al., 2017; Schmidt and Kofuji, 2009). For all experiments, 1 cell was recorded from each piece of retina with the exception of voltage-clamp experiments measuring melanopsin-mediated responses to 10 s and 100ms light stimuli, where up to 3 cells were recorded from each piece. For these experiments, the retina was dark adapted for at least 10 min before recording from the next cell. Importantly, the size of the melanopsin-mediated current was quite consistent across cells, in line with previous reports of low variability in ON alpha RGC biophysical properties (Hu et al., 2013; O'Brien et al., 2002).

Recordings were made using fire-polished borosilicate pipettes (Sutter Instruments, 3-5 M Ω for M4 cells, 5-8 M Ω for M1 cells). A Multiclamp 700B amplifier (Molecular devices) was used with pClamp 10 acquisition software (Molecular devices). All reported voltages are corrected for a -14 mV liquid junction potential calculated using Liquid Junction Potential Calculator in pClamp. Cells were bridge balanced in all current clamp recordings that required current injections.

For nucleated patch recordings, constant negative pressure was applied after gaining whole-cell access. Then, the pipette was slowly retracted from the cell, which took 5-10 min on average. The cell was discarded if the holding potential became unstable during the retraction process or if the resting membrane potential of the nucleated patch was unstable or significantly depolarized (>-40 mV). 20 μ M L-AP4 and 500 nM TTX were added to AMES' medium to improve holding current stability. Current clamp recordings were utilized for pharmacology experiments in the nucleated patch configuration because the currents measured in voltage clamp were very small.

Viral Infection

Mice (P30-60) were anesthetized by intraperitoneal injection of 2,2,2-Tribromoethanol and placed under a dissection microscope. A 30 gauge needle was used to puncture a hole through the ora serrata. Each eye was then injected with 1 μ L of AAV2/hSyn-DIO-hM3D(Gq)-mCherry (4.6×10^{12} viral particles/mL, Roth Lab via UNC Vector Core) using a custom Hamilton syringe with a 33 gauge needle (Borghuis Instruments). Retinal recordings were performed 1-2 weeks after infection and 10 nM clozapine N-oxide (CNO, Tocris) was bath applied to activate DREADDs. 10 nM was empirically determined as the concentration of CNO that elicited the same amount of depolarization in M4 cells as the intrinsic melanopsin response to bright (12 log quanta/cm²/s) background light (Figure 2). Experiments using 100 pM CNO were performed with a new batch of AAV2/hSyn-DIO-hM3D(Gq)-mCherry (4×10^{12} viral particles/mL, Addgene viral prep #44361-AAV2).

Immunohistochemistry

After recording, retinas were fixed in 4% paraformaldehyde (Electron Microscopy Sciences) in 1X PBS overnight at 4°C. Retinas were then washed in 1X PBS for 1 hr at room temperature (RT) and transferred to blocking solution (2% donkey serum in 0.3% Triton PBS) for at least 2 hr at RT. Retinas were then transferred to primary antibody solution containing either goat anti-choline acetyl transferase (ChAT, 1:500, Millipore) or mouse anti-SMI-32 (1:500, BioLegend) in blocking solution for 2-4 days at 4°C. Then, retinas were washed in 1X PBS for 3x20 min and transferred to secondary antibody solution containing, Streptavidin conjugated with Alexa 488 (1:500, Thermo) and Alexa 546 donkey anti-goat (1:500, Thermo) or Alexa 647 donkey anti-mouse (1:500, Thermo) in blocking solution for 3-4 hr at RT. Retinas were then washed in 1X PBS for at least 1 hr at RT and mounted using Fluoromount aqueous mounting medium (Sigma).

QUANTIFICATION AND STATISTICAL ANALYSIS

All data were analyzed offline using custom scripts written in MATLAB (MathWorks). Spike responses to drifting sine-wave gratings (2 cycles/s) were binned in 50ms bins. A Fourier transform of these data were then taken and the fundamental (F1) amplitude was converted to spikes/second. Then, F1 amplitude versus contrast data were fit using a hyperbolic function (Albrecht and Hamilton, 1982):

With ' R_{\max} ' being the maximum response and ' C_{50} ' being the contrast that evoked 50% maximal response. Contrast gain was calculated as the slope of this function at 20% of the maximum response (Grubb and Thompson, 2003).

$$Response(contrast) = R_{\max} \left(\frac{(contrast)^n}{(contrast)^n + C_{50}^n} \right)$$

Because the contrast response function did not always saturate, the fit was constrained between 0 spikes/s and the maximum response (R_{\max}) of each cell to more accurately measure C_{50} and contrast gain over the range of contrasts presented (Grubb and Thompson, 2003; Sarnaik et al., 2014).

Steady-state firing was measured in loose-patch recordings from M4 cells by calculating the average firing rate 1 min prior to presentation of drifting sine-wave gratings used to measure contrast sensitivity. To measure resting membrane potential of cells at dim and bright light levels, cells were first allowed to stabilize in the dark for approximately 3 min following break in. Then, cells were exposed to 5-10 min of background light. Cells reached a steady-state membrane potential within 5 min of exposure to background

light (Figure S2). To calculate resting membrane potentials in the dark, the membrane potential of the cell was averaged 30 s prior to the onset of background light. To calculate resting membrane potentials in background light, the average membrane potential was calculated over a 1 min window after at least 5 min of background light exposure.

In experiments measuring the intrinsic excitability of M1 and M4 cells, cells were held at a subthreshold voltage of approximately -75 mV followed by a series of 1 s depolarizing current steps. The current required to hold M4 cells at -75 mV in synaptic blockers ranged from -40 to $+30$ pA in darkness and from -150 to -80 pA in bright ($12 \log$ quanta/cm²/s) background light. The total number of spikes in response to each current injection was counted to construct a current-firing rate relationship.

For voltage clamp experiments measuring the maximum intrinsic response evoked by a 10 s light pulse, cells were voltage clamped between -120 and 40 mV (M4 cells) and -80 and 40 mV (M1 cells) and allowed to stabilize at these command voltages for 1-3 min prior to light stimulation. Only a single cell was recorded per command potential because cells often did not return to their baseline holding current after light offset. In cases where the holding current returned to baseline, the recovery took more than 10 min (Figure S5). The maximum change in current was calculated by averaging 50ms around the point with the greatest change from baseline during the recording period. Values are reported in absolute current (pA) because capacitance did not differ in WT M4 cells collected across different voltages in Figures 7C and 7D and in nucleated TRPC 3/6/7 KO M4 cells in Figures 7E and 7F. The capacitance of intact WT and TRPC 3/6/7 KO M4 cells was also similar (data not shown).

For experiments measuring single action potential waveforms, cells were held at ~ -74 mV and a series of 1ms current injections were made in 50 pA steps. The first evoked action potential was used for analysis. Action potential half-width was measured by measuring the width of the action potential at half-maximal amplitude (measured from baseline). Threshold was calculated from the first derivative of the voltage trace and by measuring the point which deviated 4 standard deviations above baseline. Afterdepolarization (ADP) amplitude was measured relative to baseline.

For unpaired statistical comparisons, we used a non-parametric, two-tailed Mann-Whitney U test with a Bonferroni correction. For paired statistical comparisons, we used a non-parametric, two-tailed Wilcoxon matched-pairs signed rank test. Statistical comparisons were made using Graphpad Prism 6. Significance was concluded when $p < 0.05$.

DATA AND SOFTWARE AVAILABILITY

Requests for custom scripts and raw data can be directed to the Lead Contact, Tiffany Schmidt (tiffany.schmidt@northwestern.edu).